Developing radioimmunotherapy for osteosarcoma using comparative oncology

A Thesis Submitted to the
College of Graduate and Postdoctoral Studies
In Partial Fulfillment of the Requirements
For the Degree of Master of Science
In the College of Pharmacy and Nutrition
University of Saskatchewan
Saskatoon

By
Jaline Broqueza

Permission to Use

In presenting this thesis/dissertation in partial fulfillment of the requirements for a Postgraduate degree from the University of Saskatchewan, I agree that the Libraries of this University may make it freely available for inspection. I further agree that permission for copying of this thesis/dissertation in any manner, in whole or in part, for scholarly purposes may be granted by the professor or professors who supervised my thesis/dissertation work or, in their absence, by the Head of the Department or the Dean of the College in which my thesis work was done. It is understood that any copying or publication or use of this thesis/dissertation or parts thereof for financial gain shall not be allowed without my written permission. It is also understood that due recognition shall be given to me and to the University of Saskatchewan in any scholarly use which may be made of any material in my thesis/dissertation.

Requests for permission to copy or to make other uses of materials in this thesis/dissertation in whole or part should be addressed to:

Dean of the College of Pharmacy and Nutrition
107 Wiggins Rd
University of Saskatchewan
Saskatoon, Saskatchewan S7N 5E5 Canada

OR

Dean of the College of Graduate and Postdoctoral Studies
University of Saskatchewan
116 Thorvaldson Building, 110 Science Place
Saskatoon, Saskatchewan S7N 5C9, Canada

Abstract

Osteosarcoma (OS) is one of the most common primary malignant bone cancer in children wherein the mortality rate within 5 years is 30% and patients suffer from bone pain, limited or loss of limb function, or fatigue. In addition, OS is one of the most widespread cancers in companion dogs, particularly larger breeds, and closely resembles human OS. Unfortunately, in over 30 years, there has been no significant advancement in treatment options in humans; and canine treatment options are also limited. The cation independent mannose-6- phosphate/insulin-like growth factor-2 receptor (IGF2R) was found to be consistently overexpressed on multiple standard OS cell lines, including patient-derived xenografts, as well as on tumors from dogs with OS, making it a promising therapeutic target for radioimmunotherapy (RIT). RIT involves the use of an antibody labeled with an alpha- or beta- emitting radioisotope which delivers cytotoxic radiation to targeted cells. Our objective is to develop a novel, effective and safe treatment for OS using RIT using a comparative oncology approach. Antibodies against IGF2R were developed using phage-display, a combinatorial protein engineering technique wherein bacteriophages are used to select for high affinity reagents. The IGF2R-specific antibodies were tested in vitro by performing ELISA and flow cytometry and were also tested *in vivo* by performing microSPECT/CT imaging which confirmed that the antibody bound to the OS tumors in mice. This was followed by therapy studies which involved the testing of the IGF2R-specific antibody radiolabeled with Lutetium-177, a β-emitting theranostic radioisotope, for therapeutic efficacy studies in mouse models of human and canine OS. Future studies will involve a clinical trial in canine OS patients. The development of IGF2R-specific RIT will lead to a better therapeutic strategy for not only human OS but also for canine OS and will pave the way to increase survival for OS patients.

Acknowledgements

I would like to first express my sincere and deep gratitude to my supervisor, Dr. Ekaterina (Kate) Dadachova, for providing me a compelling project, for giving me an opportunity to develop and learn research-related skills, for being patient and supportive throughout my Masters program. Her kindness, guidance and motivation helped me gain confidence in myself and my research and have been an essential part in the completion of this thesis.

I would also like to express my deepest appreciation to my co-supervisor, Dr. Maruti Uppalapati, for his continual support, for helping me understand research, and for his continuous encouragement. His critical thinking skills made me more aware of the qualities I should develop to become a better researcher.

My sincere thanks to all my committee members, Dr. Ryan Dickinson, Dr. Valerie MacDonald-Dickinson, and Dr. Ildiko Badea for their valuable feedback and knowledge they have shared throughout my research work.

I would like to give my heartfelt thanks to my lab members, Hanan Babeker, Chandra Bose Prabaharan, Mackenzie Malo, Dr. Kevin Allen, Dr. Rubin Jiao, Dr. Ravendra Garg, Dr. Wojciech Dawicki, and Connor Frank, for all their help and valuable advice during my research program. Their support and guidance have been an integral part of this thesis.

My deepest thanks to the College of Pharmacy and Nutrition at the University of Saskatchewan, the staff of the Fedoruk Centre and the Lab Animal Services Unit for providing the facilities and assistance throughout my experimental work. I would like to thank the Canadian Institutes for Health Research (CIHR) for funding this project.

I would also like to take this opportunity to thank my friends who have been supportive and have believed in me since I started my pursuit for research. Finally, I would like to thank my parents and my sister, for supporting me and believing in me.

Table of Contents

List of Tables

List of Figures

List of Abbreviations

OS	Osteosarcoma
WHO	World Health Organization
IGF2R	Insulin-like Growth Factor 2 Receptor
RIT	Radioimmunotherapy
IF1	IGF2R IgG1 antibody from Fab-1
IF2	IGF2R IgG1 antibody from Fab-2
IF3	IGF2R IgG1 antibody from Fab-3
TRT	Targeted radionuclide therapy
mAb	Monoclonal antibody
IgG	Immunoglobulin G
Fab	Antigen-binding fragment
CT	Computed tomography
microSPECT	micro Single photon emission computed tomography
SG-iTLC	Silica gel instant thin layer chromatography
ATCC	American Type Culture Collection
CPM	Counts per minute
%ID/G	Injected dose per gram percentage
HPLC	High-performance liquid chromatography
Fab	Antigen-binding fragment
SNP	Single nucleotide polymorphism
SRS/SRT	Stereotactic Radiation

FDA	Food and Drug Administration
CDR	Complementary determining region
SCID	Severe combined immunodeficient mice
PBS	Phosphate buffered saline
VL	Variable light chain
VH	Variable heavy chain
FBS	Fetal Bovine Serum
PDX	Patient Derived Xenografts
PD	Patient-derived
IP	Intraperitoneal
IV	Intravenous
^{177}Lu	Lutetium-177
^{188}Re	Rhenium-188
^{111}In	Indium-111
WBC	White blood cells (Leukocytes)
RBC	Red blood cells (Erythrocytes)
MALDI	Matrix-assisted laser desorption/ionization
HPLC	High Performance Liquid Chromatography
CIHR	Canadian Institutes of Health Research
MTD	Maximum Tolerated Dose
IGF-II	Insulin-like growth factor II
FcRn	Neonatal fragment crystallizable-receptor
Fc	Fragment crystallizable region

TMDD	Target-mediated drug disposition
FACS	Fluorescence-activated cell sorting

1.0 INTRODUCTION

Osteosarcoma (OS) is one of the most common primary malignant bone tumor wherein its incidence is more prevalent in children and adolescents. The overall 5-year survival rate of individuals with OS is approximately 60% ("Osteosarcoma - Childhood and Adolescence: Statistics", 2021) and those with metastatic disease have much poorer outcomes (Mirabello *et al*., 2009; "Osteosarcoma - Childhood and Adolescence: Statistics", 2021). Moreover, OS survivors still suffer from general health related issues, chronic medical condition, and permit life-long follow-ups for second malignant neoplasms (Nagarajan *et al,* 2011). In addition, OS is one of the most widespread cancers in large breed companion dogs and closely resembles human OS wherein gross and histopathologic architecture are comparable and similar metastatic rates and origin of the cancer are observed.(Mueller *et. al.*, 2007; Simpson *et al,* 2017). Unfortunately, in over 30 years, there has been no significant advancements in finding new treatment options for OS and canine treatment options are also limited. Although therapies such as chemotherapy and radiation therapy are available and have reasonable efficacy, patients' response rate and survival time are variable and can be difficult to predict. Moreover, OS has a broad genetic variability from one tumor to the next (Czarnecka *et al.*, 2020), making it challenging to pursue conventional therapies.

Targeted radionuclide therapy (TRT) is a type of therapy which involves a radioactive drug that targets specific cells with high precision and delivers cytocidal radiation in the form of alpha- or beta- emitting radionuclides. TRT also avoids side effects of external beam radiation therapy (EBRT) in which healthy cells surrounding the affected area are also destroyed. Radioimmunotherapy (RIT) is a subset of TRT, which uses antibodies as the delivery agent of cytotoxic radionuclides towards the target cells.

Cation independent mannose-6-phosphate/insulin-like growth factor-2 receptor

(M6PR/IGF2R) is a receptor that was found to be consistently overexpressed on multiple standard and patient-derived OS cell lines as well as on canine OS tumors making it a promising therapeutic target for RIT (Hassan *et al.*, 2012; Geller *et al*, 2016; Karkare *et al.*, 2019). A study published in 2016 has shown promising results using RIT in treating OS mouse xenograft models (Geller *et al.*, 2016). In this study, the mouse monoclonal antibody (mAb), MEM-238, which targets human IGF2R, was radiolabeled with Rhenium-188 (^{188}Re), a beta-emitting radionuclide. Suppression of the tumor growth was observed in animals treated with RIT compared to the untreated ones. Moreover, another study published in 2019 (Karkare *et al,* 2019) has shown the same result with a different antibody, 2G11, that is cross-reactive with both human and murine IGF2R. The 2G11 mAb was radiolabeled with Lutetium-177 (^{177}Lu), a beta-emitting radioisotope, and has shown that RIT significantly slowed down the growth of human OS tumors in mice without significant local and systemic toxicity.

As we progress towards developing a new form of treatment for OS, our goal is to develop a fully human IGF2R-specific mAbs that are cross-reactive to human, murine and canine versions of the IGF2R protein. This will allow a comparative oncology approach for simultaneous development of RIT for both human and canine patients. A sequence alignment of the human, murine, and canine IGF-II ligand binding region showed that this region is highly conserved among these species with 82% sequence identity (Broqueza *et al*, 2021). The IGF2R-specific human antibodies for this project were developed using phage-display, a combinatorial protein engineering technique wherein bacteriophages are used to select for high affinity reagents. The IGF2R-specific antibodies were radiolabeled with Indium-111 (^{111}In) for micro-single photon emission computed tomography (SPECT)/computed tomography (CT) imaging to confirm accumulation of antibody in OS tumors *in vivo.* This was followed by therapy studies with the

therapeutic radionuclide, ^{177}Lu, which involved the testing for therapeutic efficacy in mouse models of human and canine OS.

This project aims to develop a novel treatment for OS based on RIT, by generating IGF2R-specific monoclonal antibodies using the phage-display technique and using the comparative oncology approach. This will lead to new strategies to treat not only human OS but also OS of our non-human family members as well.

2.0 LITERATURE REVIEW

2.1 Primary Bone Cancer

Sarcoma refers to cancers that arise from tissues embryologically derived from the mesenchyme, such as the bone or in the soft tissues, also called as connective tissue, in the body. Bone sarcoma can arise in any part of any bone and begins once an accumulation of mutations, either spontaneous or induced secondary to carcinogens, is sufficient to transform healthy cells into neoplastic cells, creating a mass of tissue of abnormal cells called a tumor. A tumor may be benign or malignant. A benign tumor can grow, however, it does not spread to other parts of the body, but it can still weaken the bone and predispose a patient to a bone fracture at the site of the mass. ("Bone Cancer (Sarcoma of Bone): Introduction", 2020). An example of a benign bone tumor is osteoma which typically forms on the skull but can also develop on the long bones of the body such as the femur and tibia. A malignant tumor, on the other hand, can spread to other parts of the body through a process known as metastasis. An example of metastatic tumor is osteosarcoma.

Primary bone sarcoma is a cancer that originates from the cells of the bone itself, which mainly comprises of osteoblasts. It does not include cancer that has metastasized and occurs

more often in male than female where it has been estimated that 2100 male and 1510 females will be diagnosed with primary bone sarcoma in the United States in the year 2021 ("Bone Cancer (Sarcoma of Bone): Statistics", 2021). Patients suffering from primary bone sarcoma have an increased chance of getting a bone fracture as local tumor growth of the cancer leads to the destruction of the adjacent normal bones.

There are different types of primary bone sarcomas which includes chondrosarcoma, chordoma. Ewing's sarcoma, and osteosarcoma (Table 2.1).

Table 2.1. 5-year survival rate (%) of patients with primary bone sarcoma. Information gathered from "Bone Cancer (Sarcoma of Bone): Statistics", 2021.

		5-year survival rate (%)			
Bone Cancer Type	**Definition**	**Overall**	**If cancer is diagnosed at a localized stage**	**If cancer has metastasized to surrounding tissues/organs**	**If cancer has metastasized to distant parts of the body**
Chondrosarcoma	cancer of the cartilage	78	91	75	22
Chordoma	cancer of the tissue in the spinal cord	82	87	83	55
Ewing's sarcoma	cancer that develops in the bone or soft tissue	62	82	67	39
Osteosarcoma	cancer of bone-forming cells	60	74	66	27

For OS, the World Health Organization (WHO) has divided the histological classification of bone tumors into central, intramedullary, and surface tumors. Each group has its subtypes. An example of this is conventional OS which is a subtype of central OS and represents 80% of all OS cases in children and adolescents (Misaghi *et al,* 2018). Conventional

OS can further be subdivided into osteoblastic, fibroblastic, and chondroblastic groups depending on the principal features of the cell. Another subtype which falls under the classification of surface OS is parosteal OS which is a low-grade OS that arises from the periosteum and represents 4-6% of OS (Misaghi *et al,* 2018).

2.2 Osteosarcoma

Osteosarcoma (OS) is a primary bone tumor which develops from neoplastic/malignant transformation of osteoblasts that are typically found in variably mature stages within the lesion. Lesions most often arises in active metaphyses of the long bones such as distal femur, proximal tibia, and proximal humerus. However, the cancer can also originate in flat bones of the pelvis, skull, ribs and in the spine (Anderson *et al,* 2020).

Although primary bone cancer is rare, osteosarcoma is one of the most common primary bone sarcomas especially in children and adolescents, making up 2% of all cancers in children and 3% in teens ("Osteosarcoma - Childhood and Adolescence: Statistics", 2021). According to a study published in 2009, the incidence of OS in children and adolescents is relatively consistent around the world (Mirabello *et al*., 2009). The study found that the occurrence of OS peaked at younger ages in females in comparison to males. However, in most countries, OS was more common in males than females. Moreover, from 1973 to 2004, the incidence of the bone cancer was found to be increased in the youngest age group, variable in middle age group and decreased in the elderly (Mirabello *et al*., 2009).

The cause of OS is still unknown but there are some risk factors that increases a person's chance of getting the disease such as hereditary disorders including but not limited to retinoblastoma, Li-Fraumeni syndrome, and Werner syndrome (Ritter and Bielack, 2010;

"Osteosarcoma - Childhood and Adolescence: Risk Factors", 2021; Czarnecka, *et al,* 2020). It has also been previously shown that a single nucleotide polymorphism (SNP) within a haplotype block also increases the chances of developing OS (Savage *et al.*, 2007).

The 5-year survival rate for children with OS is 68% and decreases with the development of metastatic disease, with the rate dropping to 27% once the cancer spreads to distant parts of the body from the site of disease ("Osteosarcoma - Childhood and Adolescence: Statistics", 2021). The survival rate for OS patients depends on many different factors including the type and subtype of cancer, the time the cancer was diagnosed, the site and size of the tumor, the development of local recurrence and the cancer response to treatment (Davis *et al.*, 1994; "Osteosarcoma - Childhood and Adolescence: Types of Treatment", 2019)

2.2.1 Diagnosis and Treatment

A suspected OS evaluation starts with the patient's full history, physical examination, and plain radiographs. The first diagnostic test for detection of OS involves a preoperative imaging protocol for any suspected bone lesion which includes an X-ray of the whole bone and adjacent joint (Misaghi *et al.*, 2018). Additional tests are also a critical part of OS diagnosis and staging. Magnetic resonance imaging (MRI) can evaluate the lesion's invasion into the soft tissue and neurovascular structures. However, this test can rule out the metastases of the cancer ("Osteosarcoma: An Introduction", 2012.). A chest x-ray and chest CT scan can be done to detect lung metastases and a bone scan of the body can show the distant spread of the disease. Another test that is essential to the diagnosis of OS is the biopsy of the tumor as it provides definite characteristics of the tumor tissue which helps determine whether the tumor is high grade (highly malignant) or low grade (Misaghi *et al.*, 2018; "Osteosarcoma: An

Introduction", n.d.; "Osteosarcoma - Childhood and Adolescence: Diagnosis", 2019).

For treatment decision-making, grade is one of the most important factors. Most musculoskeletal surgical oncologists refer to the staging system adopted by the Musculoskeletal Tumor Society (MSTS) in 1980 (modified in 1986) (Anderson *et al,* 2020). There are two histologic grades for malignant tumor: low-grade and high-grade. A low-grade malignant tumor refers to tumors that recur in the same localized and has a 25% or less probability to metastasize whereas high-grade tumors have a significantly higher chances of metastasizing to different parts of the body and requires a more notable procedure or therapy (Anderson *et al,* 2020). In children, most of the osteosarcoma tumors are high-grade ("Osteosarcoma - Childhood and Adolescence: Introduction", 2019).

OS is treated with a combination of therapies which includes neoadjuvant and adjuvant chemotherapy, surgery, and radiation therapy (Misaghi *et al.*, 2018; "Osteosarcoma: An Introduction", 2012). Methotrexate with leucovorin rescue, doxorubicin, cisplatin, and ifosfamide are the four standard chemotherapy agents that are almost in all treatment regimes (Misaghi *et al.*, 2018). Dose intensity is important as well. A study published in 2009 found an increase in mortality rate in patients who waited over twenty-one days to restart chemotherapy. They suggest resuming chemotherapy within the first twenty-one days post-operation to maintain dose intensity (Imran *et al*., 2009).

Further treatment for OS is surgery which can be divided into limb salvage and amputation. Limb salvage gives 85-90% OS patients a safe methodology of treatment which includes two essential steps: 1) resection and 2) reconstruction. Resection plays a role in the elimination of the disease as it includes excision of previous biopsy sites and tract whereas reconstruction has two forms: endoprosthetic replacement wherein the design of the implants includes

modular and custom-made; and biologic replacement which includes allograft, autograft, recycled autografts, and allografts (Misaghi *et al.*, 2018). On the other hand, amputation used to be the standard surgical treatment of OS, however, it is now reserved to non-resectable tumor with soft tissue and neuromuscular contamination (Misaghi *et al.*, 2018). Moreover, some studies have shown that patient who have undergone limb salvaging have higher survival rate than people who had amputation (Grimer *et al.*, 2002).

The third treatment option is radiation therapy. However, it is not widely used in OS treatment due to its association with risk of infection, nevertheless, it is occasionally recommended when the tumor is difficult to surgically remove or residual tumors remain after surgery (Misaghi *et al.*, 2018); "Osteosarcoma: An Introduction", 2012).

2.2.2 Canine Osteosarcoma

Canine OS is one of the most widespread cancers in dogs with its incidence rates 27 times higher than in people (Simpson *et al*., 2017). It has the same phenotype as human OS in children and occurs mostly in larger breeds with the appendicular skeleton most affected.

Osteosarcoma in dogs is often painful and its signs and symptoms may be subtle. Lameness and swelling of the site of the disease are the common signs of OS. In addition, OS can lead to deformity, depending on the location of the tumor (Ehrhart *et al,* 2013). Canine patients suffering from OS are also at risk of pathological fractures due to lesion-related bone destruction (Poon *et al,* 2020)

To diagnose OS in canine, veterinarians take radiographs of the suspected primary site and perform physical examinations. Definitive diagnosis may be obtained by performing fine needle aspiration which involves suctioning a sample of tissue directly from the lesion using

a syringe and analyzing them under the microscope (Stoewen and Pinard, n.d.) by a cytopathologist. A bone biopsy may be used to validate OS if the aspiration procedure is not diagnostic. Biopsy may be done as open incisional, closed needle or as a trephine biopsy (Ehrhart *et al,* 2013). An open incision biopsy can be beneficial due the large amount of sample collected, however, this can be outweighed by an increase in postsurgical complication in canine patients such as infection and hematoma formation (Ehrhart *et al,* 2013). A trephine biopsy, wherein a small piece of bone is collected with the marrow inside, is also an advantage for diagnosing a patient as it yields 93.8% accuracy rate. Nonetheless, this technique can increase the risk of creating pathologic fractures. A closed biopsy can also be an option which uses a Jamshidi needle to collect bone marrow. Jamshidi biopsy has an accuracy rate of 91.9% for detecting tumors and 82.3% accurate rate for classifying a tumor subtype (Ehrhart *et al,* 2013).

Thoracic radiographs, blood tests, and a urinalysis can also be performed to check the overall health of the dogs and to help assess if the cancer has metastasized to other parts of the body ("Bone Cancer in Dogs", n.d.). The examination of the spread of the disease is important in patient disease staging. It is difficult to detect pulmonary metastasis by radiographs and most dogs will have undetectable micro metastatic disease, leading to a poor prognosis in canine OS (Poon *et al,* 2020). Although it is difficult to determine at the time of diagnosis whether the cancer has metastasized, advanced imaging such as CT, MRI, PET/CT may be used as a tool in patient staging (Ehrhart *et al,* 2013).

Treatment of canine OS typically involves amputation of the affected limb followed by chemotherapy to help control the disease and target metastasis ("Bone Cancer in Dogs", n.d.; Stoewen and Pinard, n.d.). Many dogs cope well after amputation and most dog owners are

also satisfied with their pets' quality of life. (Ehrhart *et al,* 2013). However, amputation may not be suitable for some canine patients such as those who have concurrent neurological problems or severe arthritis ("Canine Osteosarcoma Fact Sheet,", n.d.). In the case amputation is not appropriate, limb-sparing surgery can be performed where the primary tumor is removed with marginal resection (Ehrhart *et al,* 2013). Stereotactic radiation (SRS/SRT) can also be considered if surgery is not optional due to tumor location ("What You Should Know about Osteosarcoma (Bone Cancer) in Dogs", n.d.). SRS offers the advantage of having a non-surgical procedure that delivers high dose of radiation to the tumor and sparing normal tissues. Moreover, canine patients who undergo this procedure result in a good to excellent limb function. However, SRS may not be readily available to veterinarians and there is also the case of the patient developing post irradiation pathologic fracture (Ehrhart *et al,* 2013). Nevertheless, it is still a good non-surgical limb-sparing alternative.

2.3 Radioimmunotherapy (RIT)

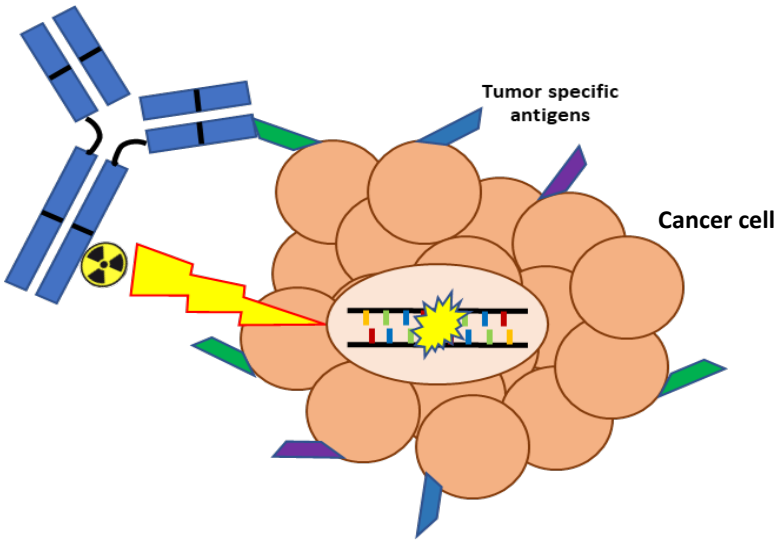

Figure 2.1. Schematic diagram of RIT.

RIT is a subset of TRT wherein an antibody is radiolabeled with an α or β - emitting radionuclide. The radiolabeled antibody delivers cytotoxic radiation to the targeted cells, killing them by damaging their DNA, making the cells unable to grow and divide. One of the advantages of RIT is that it is independent of any specific pathway. Moreover, it is not affected by resistance mechanisms or tumor microenvironmental fluctuations (Lerner, 2016; Milenic *et al.,* 2004). There are three types of radiation that are integral for TRT: photons, electrons and α-particles.

Photons are often present in the form of X-rays or γ-rays. The benefit of radionuclide photon emissions is that the photon energy is high enough to penetrate soft tissues making it ideal for imaging but insufficient to initiate double stranded DNA breaks and induce apoptosis in cells on a consistent basis which is required for therapeutic isotopes (Sgouros *et al.,* 2020). Such isotopes include technetium-99m and indium-111.

Electron emission includes Auger electrons and β-particles. Auger electrons are produced as an emission during suborbital electron transitions and are very short-ranged. They can be highly toxic to the cells if the radiopharmaceutical drug localizes in the nucleus. β-particles, on the other hand, emit electrons from the nucleus and have a longer range in tissues. β-emitters are commonly used for radiopharmaceutical therapy as they are widely available and also emit photons that can be used for imaging (Sgouros *et al.,* 2020). β-emitting isotopes include lutetium-177, yttrium-90, and iodine-131.

α-particles are helium nuclei that consists of two protons and two neutrons. They are emitted from a radioactive atom and are short-range. They are positively charged and have higher energy compared to electrons. Unlike β-particles or γ-rays, α-particles are unable to penetrate most materials and are required to be in close proximity to the target to deliver their

radioactive payload. On the other hand, their linear energy transfer, meaning the amount of energy transferred by an ionizing particle per unit distance, is 400 times greater than electrons (Sgouros *et al.,* 2020). These characteristics make α-particles a promising avenue for radiopharmaceutical therapy, with the increasing use of α-emitting radioisotopes such actinium-225 and radium-223.

Table 2.2. Partial list of therapeutic radionuclides.

Radionuclide	Therapeutic Emission	Half-life
Bismuth-213	α	46 minutes
Actinium-225	α	9.92 days
Radium-223	α	11.4 days
Astatine-211	α	7.2 hrs
Rhenium-188	β	17 hrs
Samarium- 153	β	1.9 days
Holmiun-166	β	26.8 hrs
Copper-67	β	61.83 hrs
Iodine-131	β	8 days
Ytrrium-90	β	64 hrs
Lutetium-177	β	6.65 days

Several variables should be considered for RIT such as the target antigen, the targeting antibody, and the radionuclide. An ideal target should be minimally expressed on normal cells but highly expressed at a uniform density on the surface of tumor cells. Whereas an ideal targeting antibody should penetrate tumor nodules rapidly, has high binding avidity to the target antigen, have minimal interaction with non-malignant tissues, and should be cleared from blood circulation after maximal tumor binding is achieved (Green *et al.,* 2002). In terms of radioisotopes, solid and bulky tumors can be treated with radionuclides emitting long-

ranged β particles, whereas small clusters of cancer cells can be targeted with short-ranged α-particles (Zaheer *et al.,* 2019).

Table 2.3. Partial list of radiopharmaceutical drugs currently approved by the FDA and in clinical trials. Information obtained from Sgouros *et al.,* 2020 and "FDA-approved radiopharmaceuticals", n.d.

Radiopharmaceutical	Trade name	Indication	Development-phase
Radium-223 dichloride	Xofigo	Treatment of patients with bone metastases and castration-resistant prostate cancer	FDA-approved
Gallium-68 dotatate	NETSPOTS	PET imaging for localization of somatostatin receptor positive neuroendocrine tumors	FDA-approved
Yttrium-90 ibritumomab tiuxetan	Zevalin	Treatment of Non-Hodgkin's lymphoma	FDA-approved
Lutetium-177 dotatate	Lutathera	Treatment of somatostatin receptor-positive gastroenteropancreatic neuroendocrine tumors	FDA-approved
Samarium-153 lexidronam	Quadramet	Relief of pain in patients with osteoblastic metastatic bone lesions	FDA-approved
Fluorine-18 flμCicovine	Axumin	Diagnosis of suspected prostrate cancer recurrence	FDA-approved
Fluorine-18 flutemetamol	Vizamyl	PET imaging of brain for β amyloid plaques	FDA-approved
Lutetium-177 PSMA-617		Treatment of prostate cancer	Phase III
Holmium-166		Treatment of hepatic malignancies	Phase II
Actinium-225 aCD38		Treatment of multiple myeloma	Phase I
Iodine-131 CLR 131		For paediatric cancer; Head and neck cancer; Multiple myeloma, Leukaemia, Lymphoma	Phase I

2.4 Generating monoclonal antibodies using phage-display

In addition to traditional chemotherapy and radiotherapy, targeted therapy using monoclonal antibodies (mAbs) is an effective method of therapy for several cancers (Castelli *et al.,* 2019). MAbs can be conjugated with toxins and radionuclides to improve potency. Therefore, there is immense interest in generating mAbs that bind to biomarkers of cancers in general, and specifically in our case, OS. Traditionally, antibodies are generated using the hybridoma method in mice (Doevendens and Schellekens, 2019). There are significant issues of immunogenicity due to the foreign origin of these antibodies and they often induce humoral immune response in patients. Development of murine antibodies for therapy will require extensive optimization to de-immunize these molecules through a process known as humanization (Almagro *et al.,* 2018). Recent developments in protein engineering include transgenic mice that have human immunoglobulin genes (Brüggemann *et al.,* 2015) and *in vitro* methods, such as phage-display (Fellouse and Sidhu, 2007; Lerner, 2016; Kehoe and Kay, 2005). These methods now allow for the development of human antibodies *in vitro* and *in vivo*, with theoretically no immunogenicity to human patients.

Phage-display is a combinatorial protein engineering technique where the antigen-binding fragment (Fab) regions of the antibody are expressed as a fusion coat protein of bacteriophages. Each bacteriophage virion encodes the Fab sequence in its genome and displays the corresponding Fab fragment of the antibody on its surface. A large library consisting roughly 10^{10} Fab variants, mimicking the immune repertoire, are constructed such that each virion encodes and expresses a single variant of the Fab. These constructed libraries are subsequently screened against target proteins of interest (Kehoe and Kay, 2005).

Monoclonal antibodies formats commonly used for therapy belong to the immunoglobulin G (IgG) isotype. The structure of the IgG molecule is comprised of four polypeptide chains. It consists of two identical 50 kDa heavy chain and two identical 25 kDa light chains forming a heterotetramer. These chains are usually linked by inter-chain heavy chain cysteine disulfide bonds. The heavy chains consist of an N-terminal variable region (VH) and three constant domains (CH1,CH2,CH3) whereas the light chains consist of N-terminal variable region (VL) and a constant domain (CL). The association of the light chain with the VH and CH1 domains forms the Fab region of the antibody as shown in Figure 2.2.

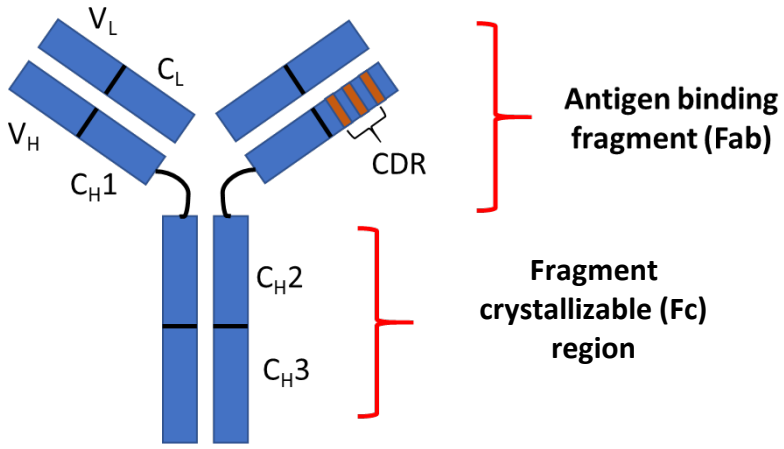

Figure 2.2. Structure of an immunoglobulin G (IgG)

The antigen binding region of the Fab consists of six complementary determining regions (CDRs). The CDRs consists of amino acid loops of different sizes and composition. The principle behind molecular recognition of target protein is the ability of a combination CDRs to form a new protein interaction interface that generates a perfect match in shape and biochemical complementarity to the target. By screening billions of potential Fab fragments in the bacteriophage library against the IGF2R protein, we expect to find Fab fragments that bind with high affinity and specificity.

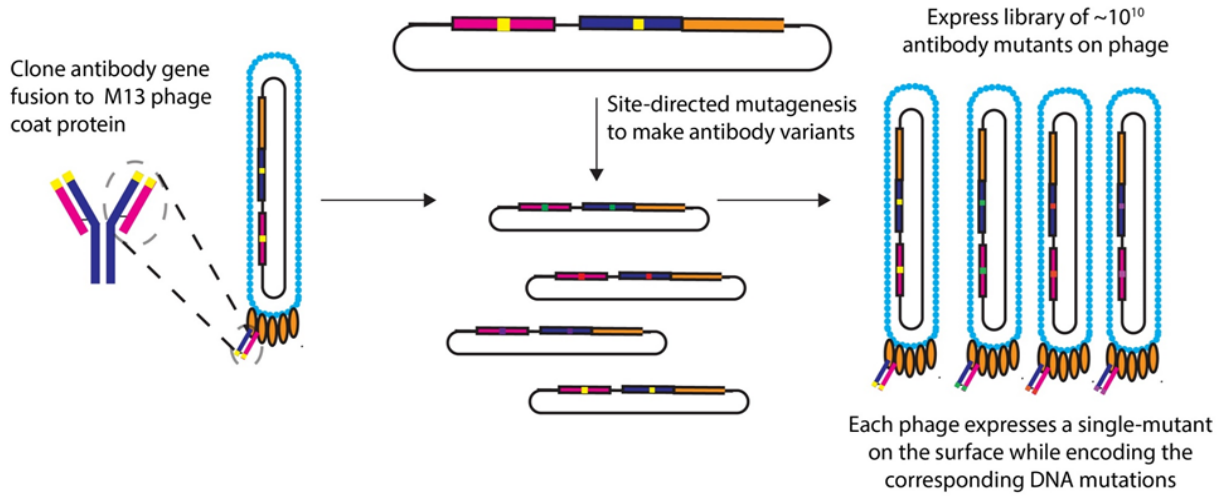

Figure 2.3. A schematic diagram of the generation of antibody libraries using phage-display technique.

To select target-specific mAbs, the library consisting of billions of variants of Fabs is used for a process called selection wherein recombinant proteins are coated on NUNC Maxisorp plates (Kehoe and Kay, 2005). For this project specifically, we generated recombinant IGF2R domains 11-14 as a soluble Fc fusion (Broqueza *et al,* 2021). The phage Fab library was depleted by allowing the phage library to bind to the Fc region of the antibody to remove non-specific binders. The unbound phage was then transferred to the plates coated with the recombinant human, murine, and canine IGF2R proteins to get IGF2R-specific binders. The bound phage antibodies were then collected, amplified and were used for the subsequent rounds of selection. Three to four rounds of selection were conducted to get Fab fragments that are highly specific and have high affinity towards the IGF2R protein from human, murine and canine origin (Broqueza *et al,* 2021).

To enable radiolabeling and subsequent use in imaging and RIT, the antibody needs to

be conjugated with a bifunctional chelator, such as CHXA", which links the antibody to the radioisotope. The isothiocyanate group of the chelator binds to the lysine residues of the antibody. Once conjugated to the antibody, the chelator acts as a claw and holds the radioisotope. Figure 2.4 demonstrates the radiolabeling of CHXA" with indium-111.

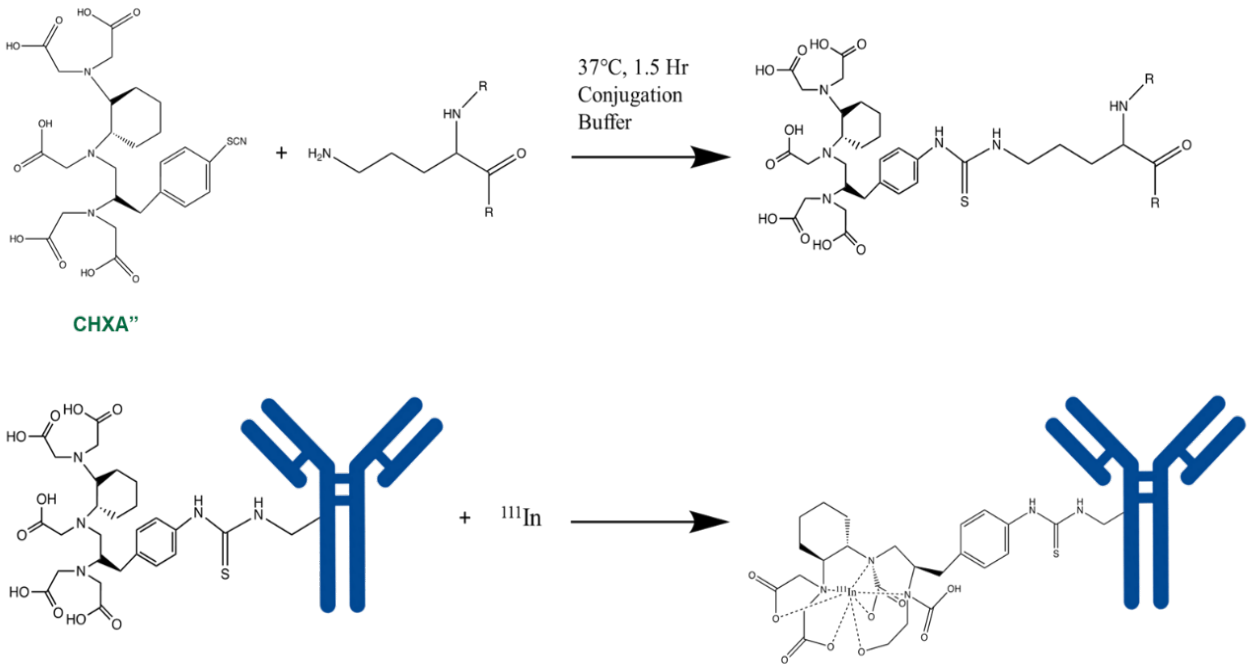

Figure 2.4. Radiolabeling of an antibody.

3.0 HYPOTHESIS AND OBJECTIVES

Hypothesis: As canine OS closely resembles human OS, we hypothesize that IGF2R-specific human antibodies can be generated that would effectively target human and canine OS tumor cells and deliver curative tumoricidal doses of radioactivity to the tumors without toxicity to normal organs.

Objectives:

1. To create a panel of IGF2R-specific human mAbs for targeting IGF2R in OS. These mAbs will be tested for their ability to bind *in vitro* to human and canine OS cell lines. The most selective antibodies will be evaluated for their ability to concentrate in OS in mouse models in Aim 2.
2. To perform microSPECT/CT imaging and biodistribution of the radiolabeled mAbs in mice bearing human and canine OS tumors. Select the antibody with the highest tumor uptake for radioimmunotherapy in Aim 3.
3. To characterize OS tumor response using radioimmunotherapy in human and canine OS tumors in mouse models and to assess the safety of such treatments.

4.0 MATERIALS AND METHODS

4.1 Reagents and Antibodies

The murine mAb, 2G11, that was used as a positive control in flow cytometry experiments was purchased from Thermofisher (Vancouver, BC, Canada). Human mAb against respiratory syncytial virus (RSV), Palivizumab, that was used as negative isotype control was obtained from MedImmune.(Gaithersburg, MD, United States). Silica gel instant thin layer chromatography (SG-iTLC) strips that was used to determine percentage labelling of the radiolabeled antibodies were acquired from Agilent (Mississauga, ON, Canada). (R)-2-Amino3-(4-isothiocyanatophenyl)propyl]-trans-(S,S)-cyclohexane-1,2-diamine-pentaacetic acid (CHXA") bifunctional chelating agent was acquired from Macrocyclics (Dallas, TX, USA). The radioisotope ^{111}In was purchased from BWXT ITG Canada, Inc. (Ottawa, ON, Canada); and ^{177}Lu from Radiomedix (Houston, TX, USA).

4.2 Cell Lines

Human OS cell line, 143B, and canine OS cell line, D17, were purchased from American Type Culture Collection (ATCC) (Manassas, VA, USA). OS-33, a well characterized patient-derived human OS cell line, was a kind gift from Dr. R. Gorlick (MD Anderson Cancer Center, Houston, TX, USA) whereas canine patient derived OS cell lines, Gracie and McKinley, were a kind gift from Dr. Doug Thamm's lab at Colorado State University School of Veterinary Medicine (Maeda *et al,* 2012). The 143B cells were cultured in Eagle's Minimum Essential medium (Hyclone, Cat. No. SH30024.01) and OS33 cells were cultured in Dulbecco's Modified Eagle Medium (Hyclone, Cat. No. SH30243.01). Both media were supplemented with 10% FBS (Hyclone, Cat. No. SH30396.03), 1% antibiotic-antimycotic Solution (100×) (Gibco, Ref. 15240-062)) and 1% MEM Non-Essential Amino Acids Solution (100X) (Gibco, Ref. 11140-050). Gracie and McKinley cells were cultured in RPMI-1640 with HEPES (Hyclone, Cat. No. SH30255.01) and was supplemented with 10% FBS, 1% antibiotic-antimycotic Solution (100×) and 1% MEM Non-Essential Amino Acids Solution (100X), and 1% sodium pyruvate (Hyclone, Cat. No. SH30239.01).

4.3 Expression of IGF2R-specific Full Length IgG_1 Antibodies in Human Mammalian Cells

The variable light chain (VL) and variable heavy chain (VH) coding sequences of the lead antibodies were cloned in pFUSE2ss-CLIg-hK vector and pFUSE2ss-CHIg-hG1 vectors respectively (Invivogen). Previously described protocol (Vazquez-Lombardi *et al*,

2018) was used to transiently express the clones in Expi293F mammalian cells. The expressed antibodies were purified by protein A affinity chromatography using MabSelectSure (GE Healthcare) affinity resin, using manufacturer recommended protocols.

4.4 ELISA of Purified IgG_1 against Recombinant IGF2R

NUNC Maxisorp 96-well plate was coated overnight with 50 ul 3 μg/ml (in 1xPBS) of recombinant human, murine and canine IGF2R, coating each well with 0.15 μg of protein. The wells were blocked with 100 μl of PB Buffer (1× PBS + 0.2% BSA) and left for one hour at room temperature. The plate was then washed twice with PT buffer (1× PBS + 0.05% Tween20). Purified IgG_1s (IF1 and IF3) diluted in PBT buffer (1× PBS + 0.2% BSA + 0.05% Tween20) were added to the corresponding wells at different concentrations ranging from 0.1 to 100 nM and was incubated at room temperature while shaking. After one hour, the plate was then washed four times with PT Buffer. Secondary antibody, Goat Anti-Human Kappa (K) Light Chain Antibody HRP (Invitrogen), was diluted (1:5000) in PBT buffer and 50 μL was added to each well and was incubated for 45 min at room temperature while shaking. After incubation, the plate was then washed with PT buffer four times. The plate was then developed with 45 μL of TMB (3,3', 5,5”-tetramethylbenzidine) substrate (1 Peroxidase Substrate: 1 TMB Peroxidase Substrate) (Seracare, Milford, MA, USA) for ~5 min. Reaction was terminated using 45 ul of 1 M Phosphoric acid and absorbance was read at 450 nm using Biotek Synergy HT.

4.5 Flow Cytometry on Human and Canine OS cells

A 96-well U-shape titration plate containing 300,000 cells in each well were incubated with the primary antibody (either 2G11, RSV, IF1, or IF3) with concentrations ranging from 3 nM to 300 nM. The cells were incubated with the primary antibody in FACS buffer (1× PBS + 0.5% BSA or 2% FBS + 0.02% azide) at room temperature for half an hour. Plate was then washed twice with FACS buffer before the addition of the secondary antibody. Goat anti-Human IgG Fc (PE) (eBioscience, cat. #12-4998-82) was used as the secondary antibody for the IF1, IF3 and RSV antibodies whereas Goat Anti-Mouse IgG2a H&L (PE) from Abcam (ab74490) was used as a secondary for 2G11. The secondary antibodies were incubated for 30 mins at room temperature. Cells were then washed again three times with FACS buffer and was then read and analyzed in the CytoFlex machine.

4.6 Animal Model

Female nude mice from Charles River Laboratories were (Wilmington, MA, USA) were used initially in pilot experiments. Female SCID (CB17/Icr-Prkdcscid/IcrIcoCrl) mice aged six-eight week old obtained from Charles River Laboratories were used for the biodistribution and therapy experiments. Mice were anesthetized with 2.5-5% isoflurane with a 1 L/min oxygen flow rate for tumor induction and were injected subcutaneously with 4 million cells of either 143B, OS33, Gracie or McKinley cells into the right flank of the mouse. Mice were monitored for weight and tumor development and were imaged or treated once tumors reached a palpable state.

4.7 Conjugation of Bifunctional Chelating Agent, CHXA", and radiolabeling of the antibodies

Before radiolabeling the antibodies, one milligram of IF1 and IF3 antibodies were conjugated with 2.5x or 10x initial excess CHXA" by loading the antibodies in 30K MW (molecular weight) Amicon Ultra 0.5 mL centrifugal filter (Millipore Sigma) and buffer exchanging into 1x conjugation buffer. To make the 1x conjugation buffer, 1 ml of 10X Conjugation Buffer buffer (0.05 M Carbonate/Bicarbonate, 0.15 M NaCl, 5 mM EDTA, pH 8.6 - 8.7) was combined with 100 µl 0.5 M EDTA, pH = 8.0 and was diluted to 10 mL with deionized water. The buffer exchange was performed by doing 10x 0.5 ml washes in a refrigerated centrifuge at 4°C at 14.0 xg for 3 minutes per spin. The antibody was recovered from the Amicon filter and fresh 2 mg/ml CHXA" was prepared by dissolving the CHXA" powder in 1x conjugation buffer. CHXA" solution was then added to the antibody to provide either 2.5-fold or 10-fold molar equivalents of CHXA". The reaction mixture was incubated at 37°C for 1.5 hours with shaking. The conjugated antibodies were then purified with 0.15 M ammonium acetate buffer (pH=6.5-7.0) by performing ten 0.5 ml washes on Amicon concentrators in a refrigerated centrifuge at 4°C. Samples were then stored at 4°C.

For the biodistribution study, antibodies were radiolabeled with Indium-111 (^{111}In) at a specific activity of 5:1 µCi/µg of the antibody. For imaging and therapy, the antibodies were conjugated at 10:1 µCi/µg specific activity. ^{111}In was used for the imaging experiments whereas Lutetium-177 (^{177}Lu) was used for the therapy study. ^{111}In or ^{177}Lu chloride was added to 0.15 M ammonium acetate buffer and conjugated antibody was added to the solution. The reaction mixture was incubated for 45 minutes at 37°C with

shaking. The reaction was then quenched by adding 3 µl of 0.05 M EDTA solution. The radiolabeling percentage was measured using SG-iTLC strips using 0.15 M ammonium acetate buffer as the solvent phase. The SG-iTLC strips were cut in half and was read on a Perkin Elmer 2470 Automatic Gamma Counter wherein the top half contains the unlabeled radioisotope and the lower half containing the radiolabeled antibody. The percentage of radiolabeling yield was calculated by dividing the counts per minute (CPM) of the bottom half by the sum of the cpm of both the top and half bottom of the strip. Radiolabeling yields were greater than 90%. To achieve 99% of the radiolabeled antibodies, the radiolabeled antibodies were purified on size exclusion spin filters by performing three washes with PBS to remove excess unlabeled isotopes. High-performance liquid chromatography (HPLC) was used to analyze the radiochemical purity of the radiolabeled antibody.

4.8 MicroSPECT/CT imaging of mice bearing Human and Canine OS tumors

Female SCID mice were subcutaneously injected with 4 million cells of either 143B, OS33, or Gracie cells. Once tumors were palpable and reached approximately 10 x 10 mm, mice were intravenously injected with 200 µCi of ^{111}In-IF3 with the radiolabeled antibody prepared using an initial 2.5 molar excess of CHXA". Mice were then imaged at the prone position at 24 and 48 hour post-injection. MILabs VECTor4 (Utrecht Netherlands) microSPECT/CT scanner was used to collect the microSPECT/CT images and was processed using the software package PMOD (version 3.9, PMOD Technologies, Inc, Zürich, Switzerland). CT data was collected for 5 minutes whereas the SPECT data was collected for 20 mins using Extra Ultra High Sensitivity Mouse (XUHS-M) collimator. All SPECT images were reconstructed with MILabs reconstruction software using both 245

keV and 171 keV ^{111}In gamma emissions on a 0.4 mm voxel grid.

4.9 Biodistribution Study

For the full-scale biodistribution study of IF1, female SCID mice bearing 143B tumors were randomized and were injected intraperitoneally with 30 μCi of ^{111}In -IF1 with a 10 molar excess of CHXA". Mice from each group were sacrificed at 24 and 72 hour post-injection and organs were collected including blood, tumor, heart, lungs, pancreas, spleen, kidney, liver, brain, stomach, small intestine, large intestine, thigh muscle and bone. Organs were weighed and radioactivity was counted in a gamma counter (Perkin Elmer, Waltham, MA, USA). The percentage injected dose per gram (%ID/g) was then calculated using a dilute standard.

For the small-scale biodistribution of IF1 vs IF3, non-bearing healthy SCID mice were injected intraperitoneally with ^{111}In -IF3 prepared with either 2.5 or 10 initial molar ratios of CHXA". Mice were sacrificed at 24 and 72 hour post injection mice from each group and blood, spleen and bone were collected, weighed, and counted in a gamma counter to calculate the percent of injected dose per gram (%ID/g) for each sample using a dilute standard.

4.10 Radioimmunotherapy Study

Female SCID mice bearing either human OS33 tumor or canine Gracie OS tumor were monitored until the tumor size reached ~50-100 mm^3. Mice were randomized into groups of five for OS33 and groups of four for Gracie. There were four therapy groups for each tumor

type. Group 1 was untreated; group 2 received unlabeled IF3 (cold: 12 ug IF3); group 3 received 80 μCi of ^{177}Lu -IF3 (8 ug, 80 μCi); group 4 received 120 μCi of ^{177}Lu -IF3 (12 ug, 120 μCi). The radiolabeled antibody used for therapy was prepared with a 2.5 initial molar excess of the CHXA". Tumors and mouse body weights were monitored three times a week and tumor volume was calculated by using the formula V= L*W^2/2. Blood was collected at the end of each week and blood counts were measured by AcT diff Analyzer (Beckman Coulter). At the completion of the study, mice were humanely sacrificed and gross pathology was performed on the animals.

5.0 RESULTS

5.1 Expression of Full-length IF1 and IF3

Three leading binders were previously developed in our laboratory against IGF2R using the phage-display technique (Broqueza *et al,* 2021). These binders are referred to as Fab-1, Fab-2 and Fab-3. Antibody constructs of the IGF2R Fab binders were expressed from mammalian vectors and was purified by affinity chromatography. Figure 5.1 shows the reduced version of the antibody wherein dithiothreitol (DTT) was added to the sample to reduce the disulfide bonds between the chains, showing the light chain at ~25 kDa and the heavy chain at ~50 kDa. The expected weight of the full length IGF2R IgG_1 antibodies is ~150 kDa. IF1 and IF3 refers to the full-length antibody from Fab-1 and Fab-3 respectively.

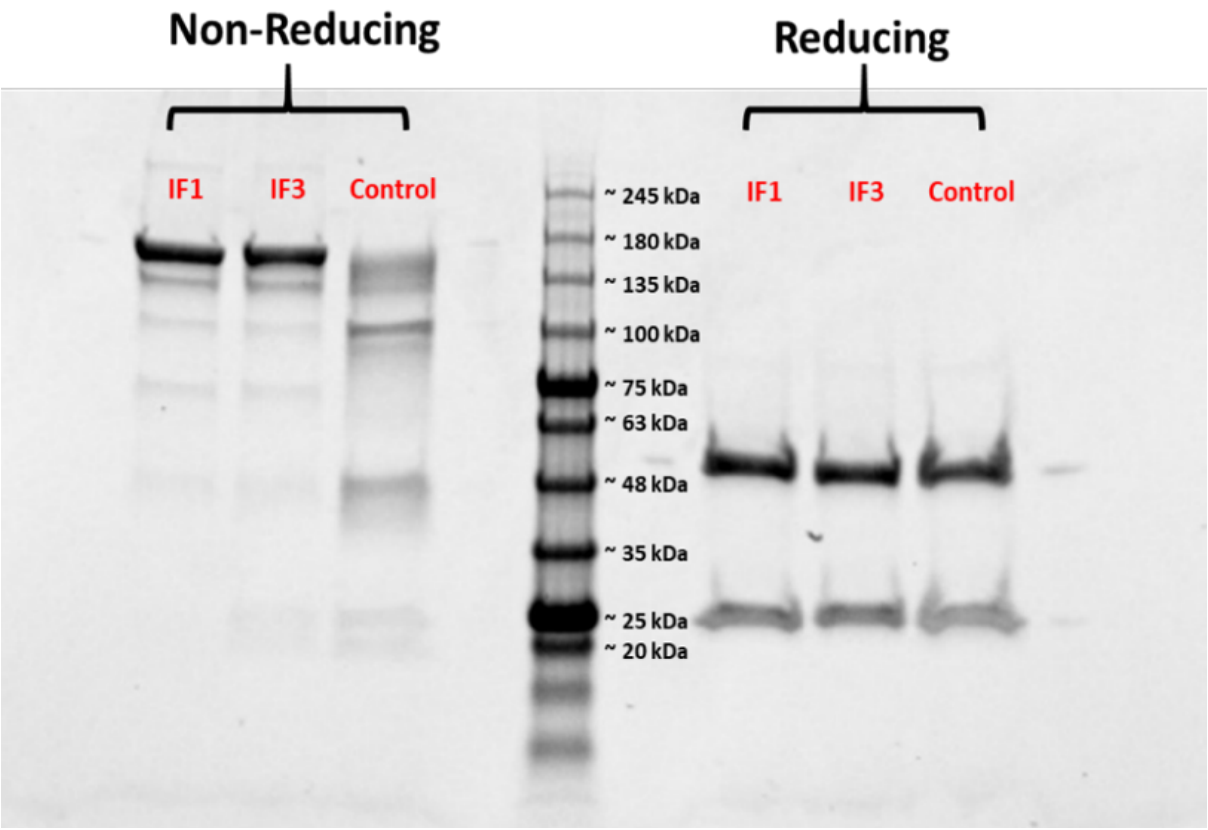

Figure 5.1. SDS-PAGE gel showing the reduced and non-reduced version of the full length IF1 and IF3 IgG_1 type antibodies to IGF2R.

5.2 ELISA of Full-length IF1 and IF3 on Recombinant Human, Canine and Murine IGF2R proteins

The expressed full length IgG_1 IGF2R-specific antibodies were validated by ELISA wherein they were tested against human, murine and canine recombinant IGF2R. Both IF1 and IF3 bound with similar affinity (EC_{50}) to human, canine and murine IGF2R.

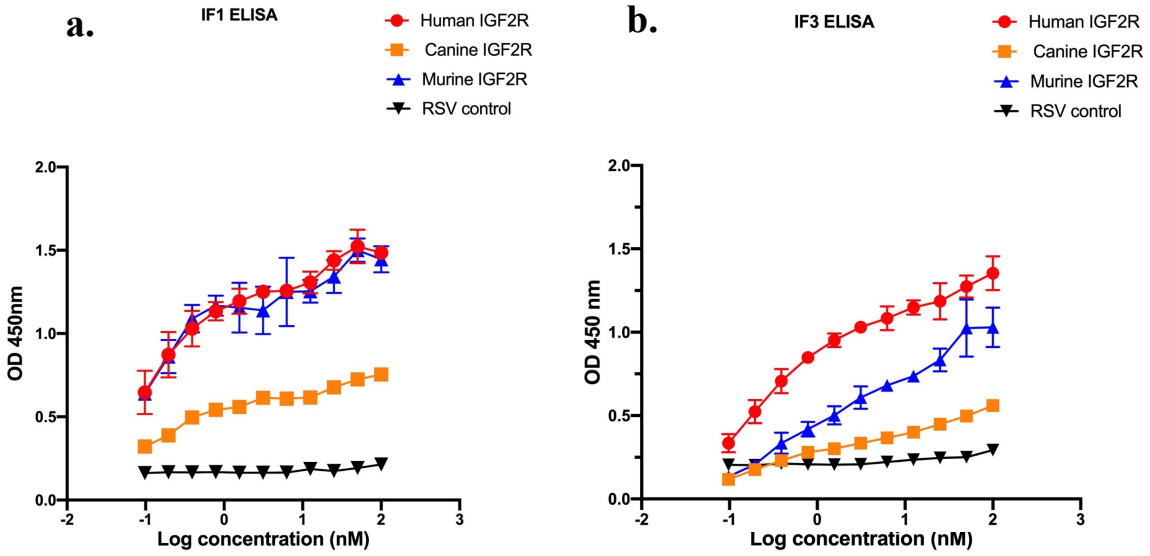

c.

	EC_{50} value (nM)	
	IF1	**IF3**
Human	1	1.1
Canine	1.4	3.2
Murine	1	3

Figure 5.2. Binding of IF1 (a) and IF3 (b) antibodies to recombinant human, canine and murine IGF2R. (c) EC_{50} values in nanomolar of IF1 and IF3.

5.3 Flow cytometry on Human and Canine OS cells with IF1

The binding of the full length IF1 antibody was tested using flow cytometry against different human and canine cell lines. 143B and D17 are human and canine commercial cell lines respectively, whereas OS33 is a patient-derived (PD) human OS cell line. Gracie and McKinley are canine PD OS cell line. Different concentrations ranging from 3 nM to 300 nM of the antibody was assessed to see if affinity of the antibodies is dose dependent. The RSV antibody (palivizumab) was used as a negative control.

A dose-dependent shift can be observed in both 143B and OS33 cells where 300 nM concentration showed a prominent shift to the right indicating that the IF1 antibody is binding to the target protein, IGF2R, expressed by these cells.

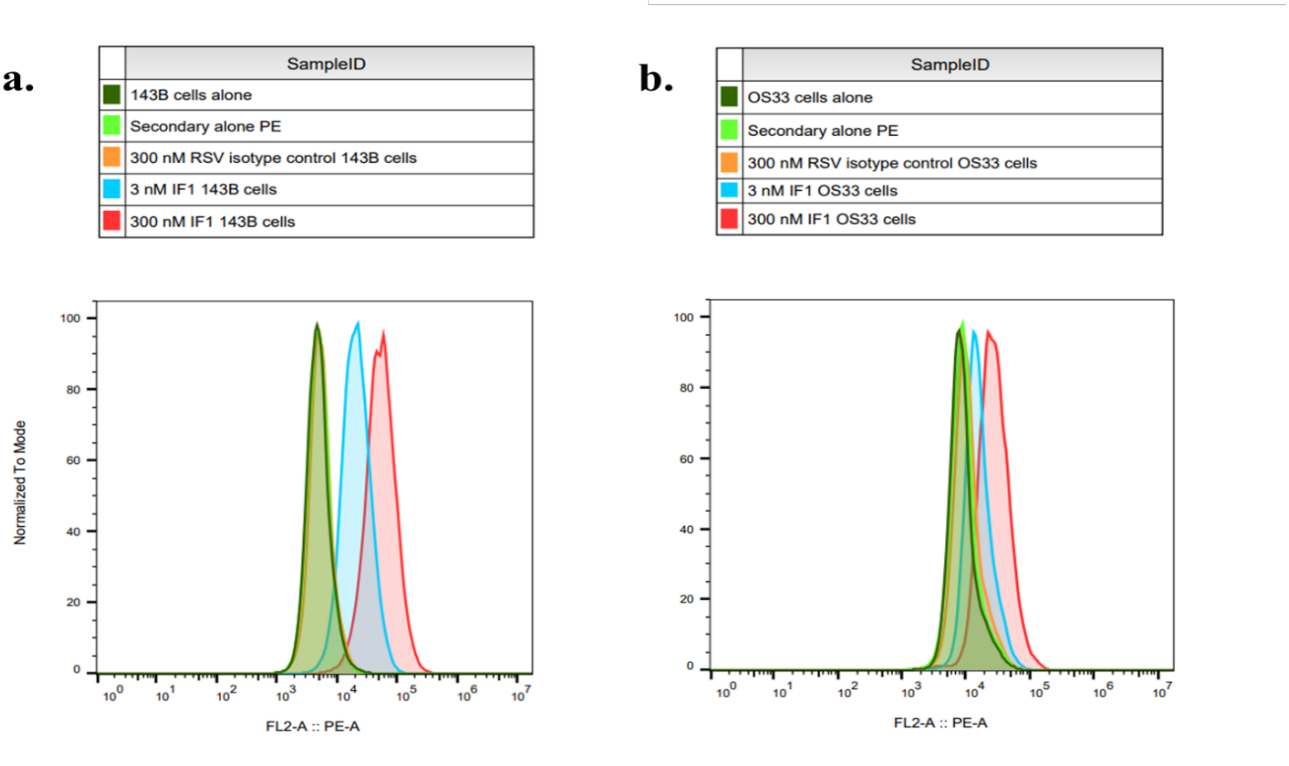

Figure 5.3. Flow cytometry on human OS cells with IF1 antibody. a.) 143B cells (commercially available) b.) OS33 cells (PD cell line)

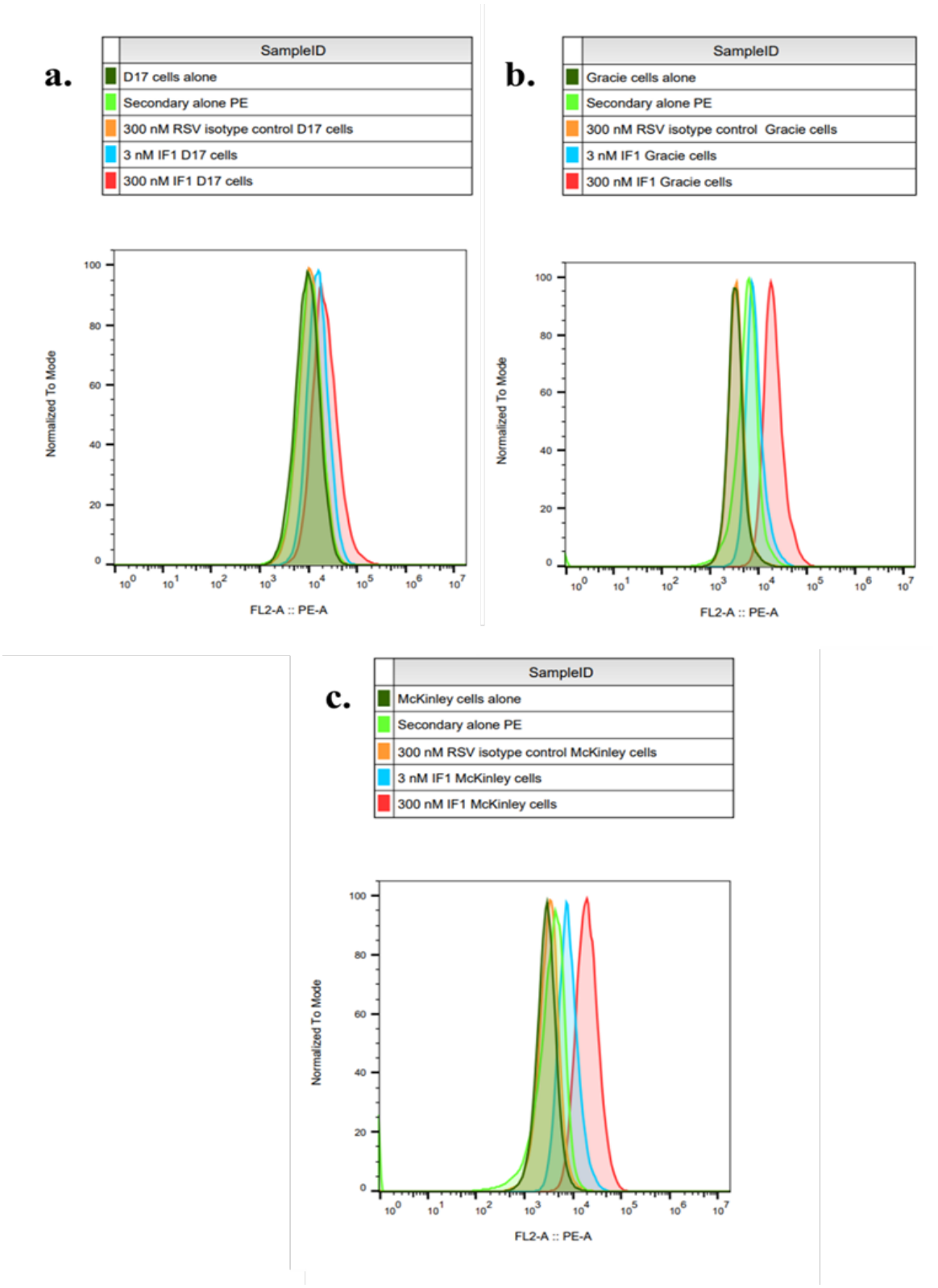

Figure 5.4. Flow cytometry on canine OS cells with IF1 antibody. a.) D17 cells (commercially available) b.) Gracie cells (PD cell line) c.) McKinley cells (PD cell line).

Dose-dependent shift can also be observed in the canine OS cells. However, the shift in the D17 cells were not significant compared to the other cells which may indicate that D17 may be expressing the IGF2R in low to moderate level.

5.4 microSPECT/CT of Indium-111 – CHXA" IF1 in tumor bearing nude mice

At the beginning of the *in vivo* experiments, nude mice were used as they are more resistant to radioactivity. OS33 or Gracie tumors were grown on the right flank of the mice. Once the tumors were palpable, mice were injected via intravenous (IV) route with 150 μCi of ^{111}In- IF1 that was conjugated with 10 times molar excess of the bifunctional chelating agent, CHXA". We used different ratios of molar excess of CHXA" during conjugation of bifunctional chelator and radiolabeling was assessed using High Performance Liquid Chromatography (HPLC). Five molar excess and twenty molar excesses of CHXA" were conjugated to the IF1 antibody and were radiolabeled with ^{111}In. Figure 5.5 shows that the 5 times molar excess of CHXA" is not optimal to get enough labelling as the second peak in the radio trace in Figure 5.5a shows that there is a significant amount of free ^{111}In left after radiolabeling which is probably in the form of ^{111}In-CHXA" complex, resulting in a yield of 68%, whereas 20 molar excess yielded to 99% labeling. However, 20 molar excess might be excessive and may affect the binding of the antibody to the target cells. Therefore, we decided to use 10 molar excess of the CHXA".

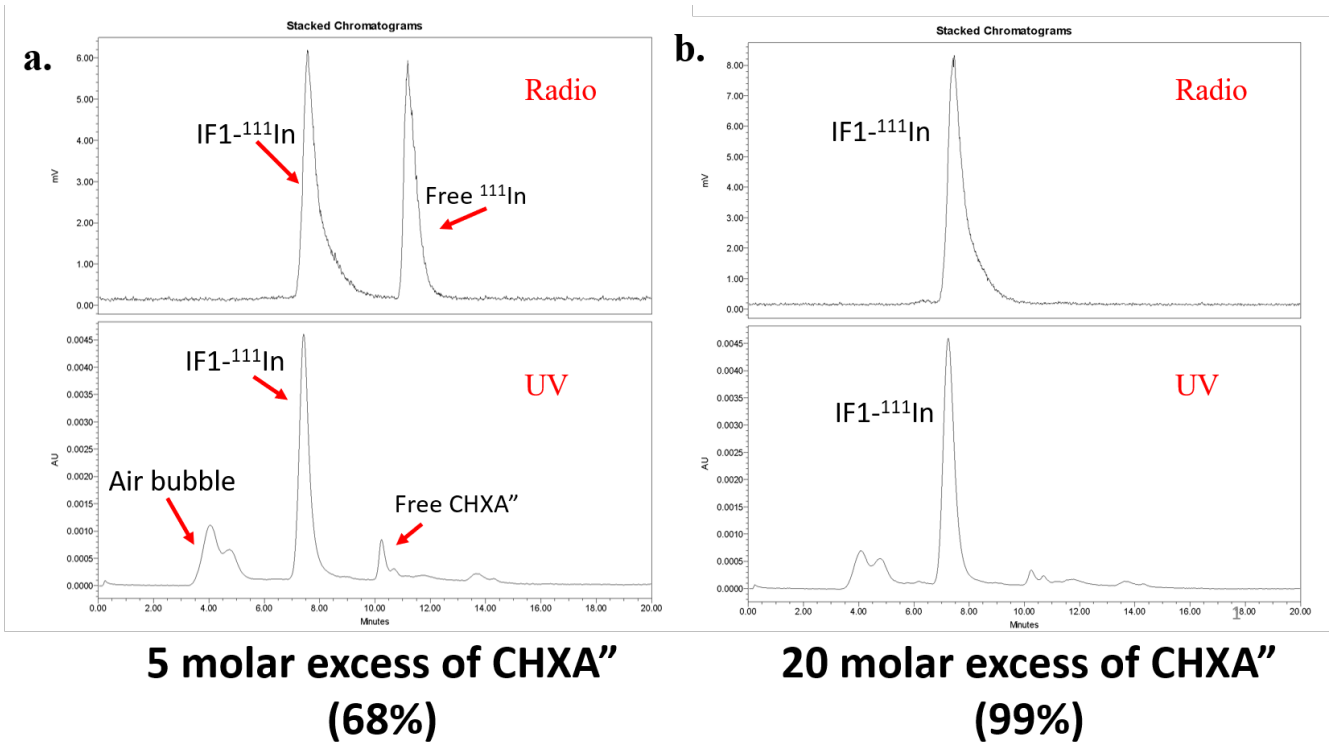

Figure 5.5. Radio-HPLC of radiolabeled ^{111}In-IF1 conjugated 5 molar excess vs 20 molar excess of CHXA"

MicroSPECT/CT was then performed on the mice injected with ^{111}In-IF1and were imaged at 24 hr, 48 hr and 7 day time point. For the 24 hr point, little radioactivity can be observed in the OS33 mouse. This may be due to a gut injection, therefore, making the antibody to be excreted out of the mouse's system fast and no opportunity for the antibody to circulate in the blood. Because of this, a different mouse, bearing the same OS33 tumor, was imaged for the 48 hr and 7-day time point. No tumor accumulation can be observed from the images, however, there is a significant spleen uptake in the mice which was also observed in a previous imaging study published in 2019 (Karkare, *et al* 2019). It is also possible that no tumor accumulation can be observed because the IGF2R expression in the tumor is suppressed by the nude mice's immune system as these mice

still have their B cells intact. Therefore, we have decided to use SCID mice for the next experiments as they are more immunocompromised since they are lacking both B and T cells.

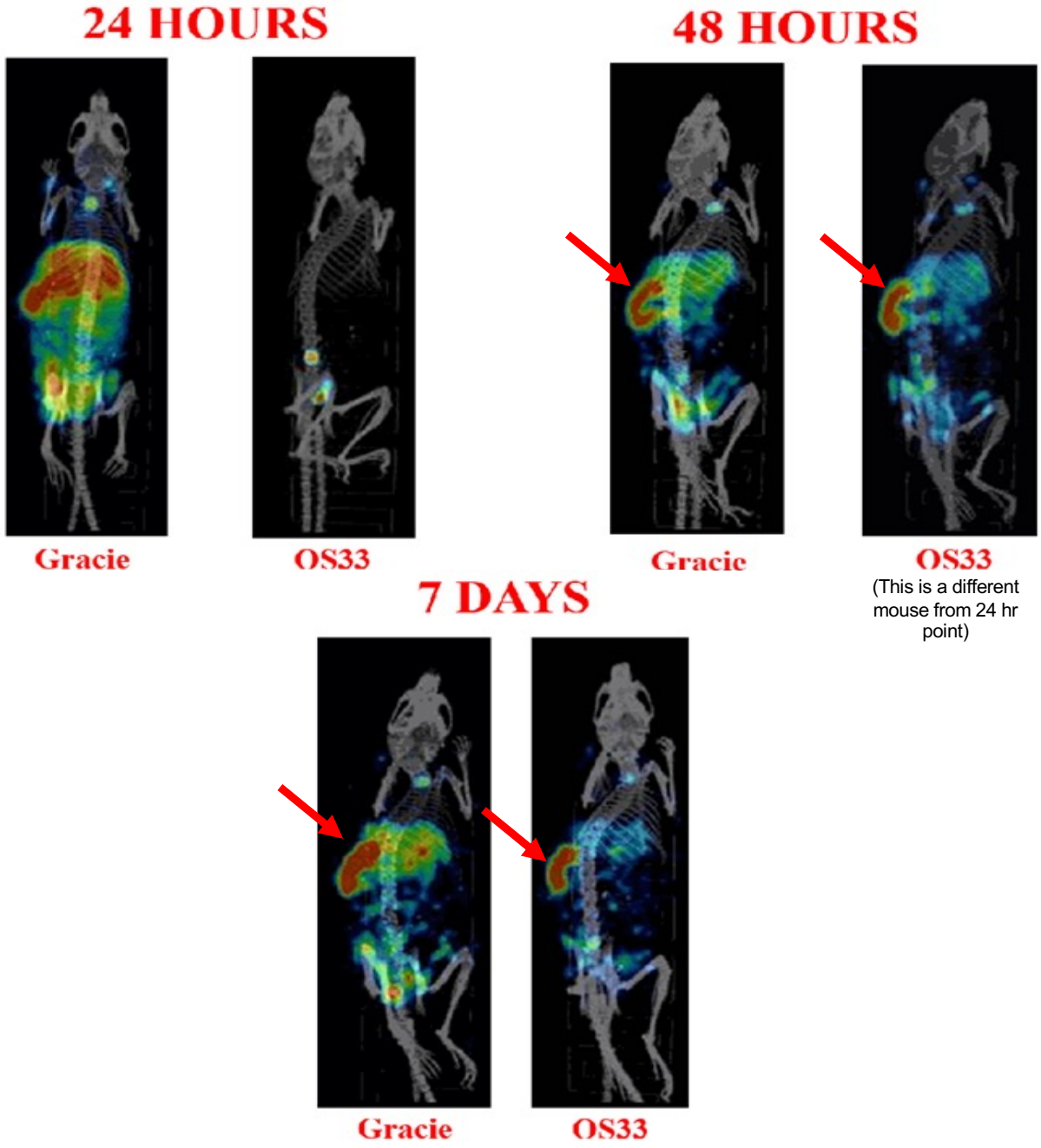

Figure 5.6. MicroSPECT/CT of tumor bearing nude mice with ^{111}In- labelled IF1. Mice were injected with either Gracie or OS33 cells and were imaged with ^{111}In- IF1 conjugated with initial 10 M excess of the CHXA" linker. Spleens are indicated by the red arrow.

5.5 Biodistribution of Indium-111-CHXA" – IF1 in 143B tumor-bearing SCID mice

Biodistribution was performed to track where the IF1 antibody uptake within the mice's organ system. SCID mice bearing 143B tumors were chosen to be the mouse model in the biodistribution as the model was used in a previous study (Karkare, *et al.* 2019). The biodistribution shows that the IF1 antibody has a fast clearance from the blood which probably affects the tumor accumulation of the radiolabeled antibody. Since the IF1 antibody does not stay in the blood for a long time, the antibody does not circulate around the body enough to give it time to accumulate in the tumor. However, the tumor specificity of IF1, which can be calculated by dividing the %ID/g (injected dose/gram) value of the blood from the tumor, shows a higher value compared to 2G11 and RSV as shown in figure 5.8.

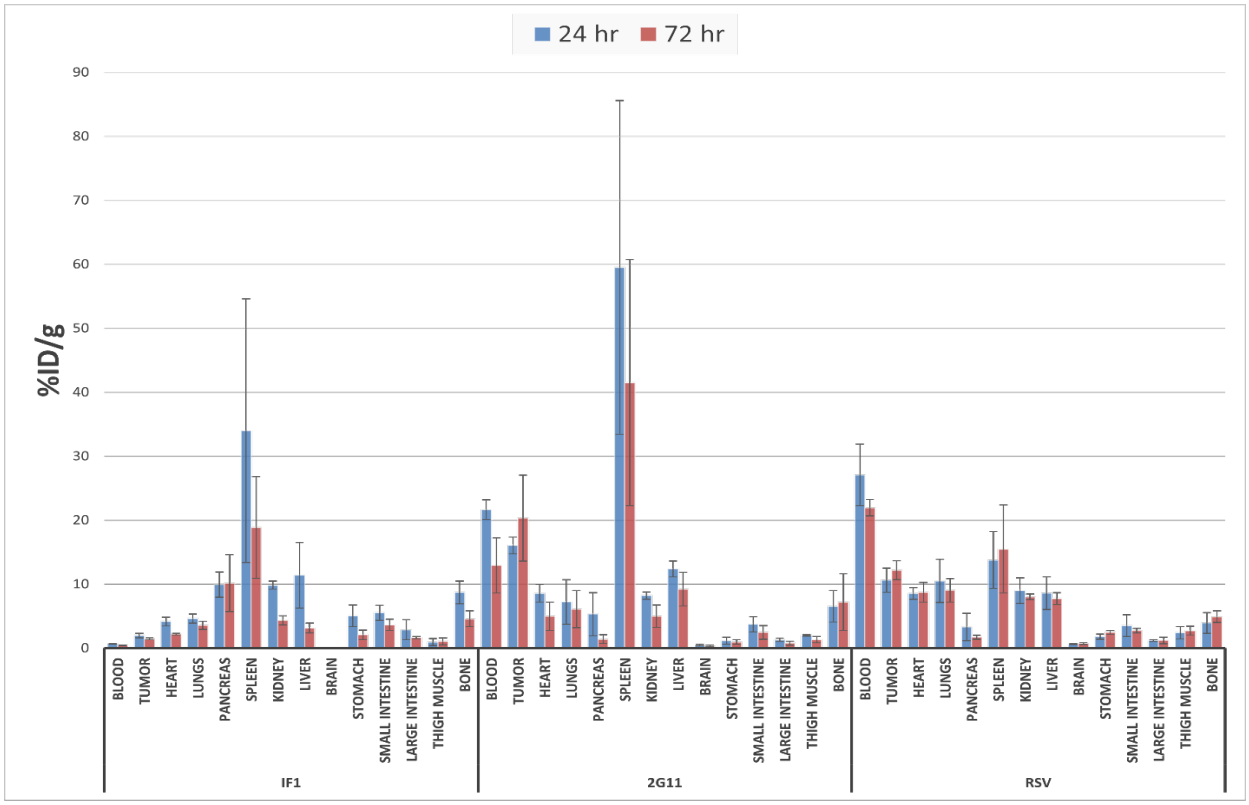

Figure 5.7. Biodistribution of ^{111}In-IF1 (6 ug, 30 µCi), ^{111}In-2G11 (Positive control, 6 ug, 30 µCi) or ^{111}In-RSV (Negative control, 6 ug, 30 µCi), antibodies in 143B tumor bearing SCID mice. All antibodies were conjugated with a 10 M excess of the CHXA" linker.

IF1

Average	Time point	
Organ	24 hr	72 hr
Blood	0.66	0.44
Tumor	1.96	1.46
Heart	4.16	2.19
Lungs	4.62	3.56
Pancreas	9.96	10.15
Spleen	33.98	18.86
Kidney	9.85	4.36
Liver	11.40	3.14
Brain	0.12	0.07
Stomach	5.04	2.07
Small Intestine	5.54	3.62
Large Intestine	2.88	1.64
Thigh Muscle	0.95	1.07
Bone	8.70	4.59

Tumor specificity	
24 hr	2.98
72 hr	3.36

2G11

Average	Time point	
Organ	24 hr	72 hr
Blood	21.66	12.92
Tumor	16.07	20.33
Heart	8.56	4.98
Lungs	7.23	6.10
Pancreas	5.32	1.41
Spleen	59.51	41.50
Kidney	8.22	5.02
Liver	12.39	9.23
Brain	0.53	0.35
Stomach	1.18	0.96
Small Intestine	3.73	2.47
Large Intestine	1.30	0.77
Thigh Muscle	2.00	1.33
Bone	6.53	7.18

Tumor specificity	
24 hr	0.74
72 hr	1.57

RSV

Average	Time point	
Organ	24 hr	72 hr
Blood	27.07	21.96
Tumor	10.64	12.17
Heart	8.55	8.74
Lungs	10.50	9.03
Pancreas	3.29	1.71
Spleen	13.77	15.48
Kidney	8.98	8.01
Liver	8.60	7.73
Brain	0.65	0.73
Stomach	1.81	2.47
Small Intestine	3.53	2.73
Large Intestine	1.20	1.20
Thigh Muscle	2.42	2.72
Bone	3.94	4.91

Tumor specificity	
24 hr	0.39
72 hr	0.55

Figure 5.8. Biodistribution of IF1 and control antibodies. % of injected dose per gram (ID/g) values of IF1, 2G11, and RSV antibodies are shown. All antibodies were radiolabeled with ^{111}In conjugated with initial 10 molar excess of the CHXA" linker.

5.6 IF3 binding to human and canine patient derived OS cells by flow cytometry

Given the lack of sufficient tumor uptake in imaging, we pursued an alternative lead antibody against IGF2R, IF3. Flow cytometry was performed to test the affinity of the IF3 antibody against human and canine OS cells. From the graph, one can confer that there is a significant shift of the IF3 antibody in all the OS cell lines, indicating that IF3 binds to the IGF2R proteins that are expressed by these cells. We have decided to test the IF3 antibody biodistribution in concurrence with IF1 *in vivo.*

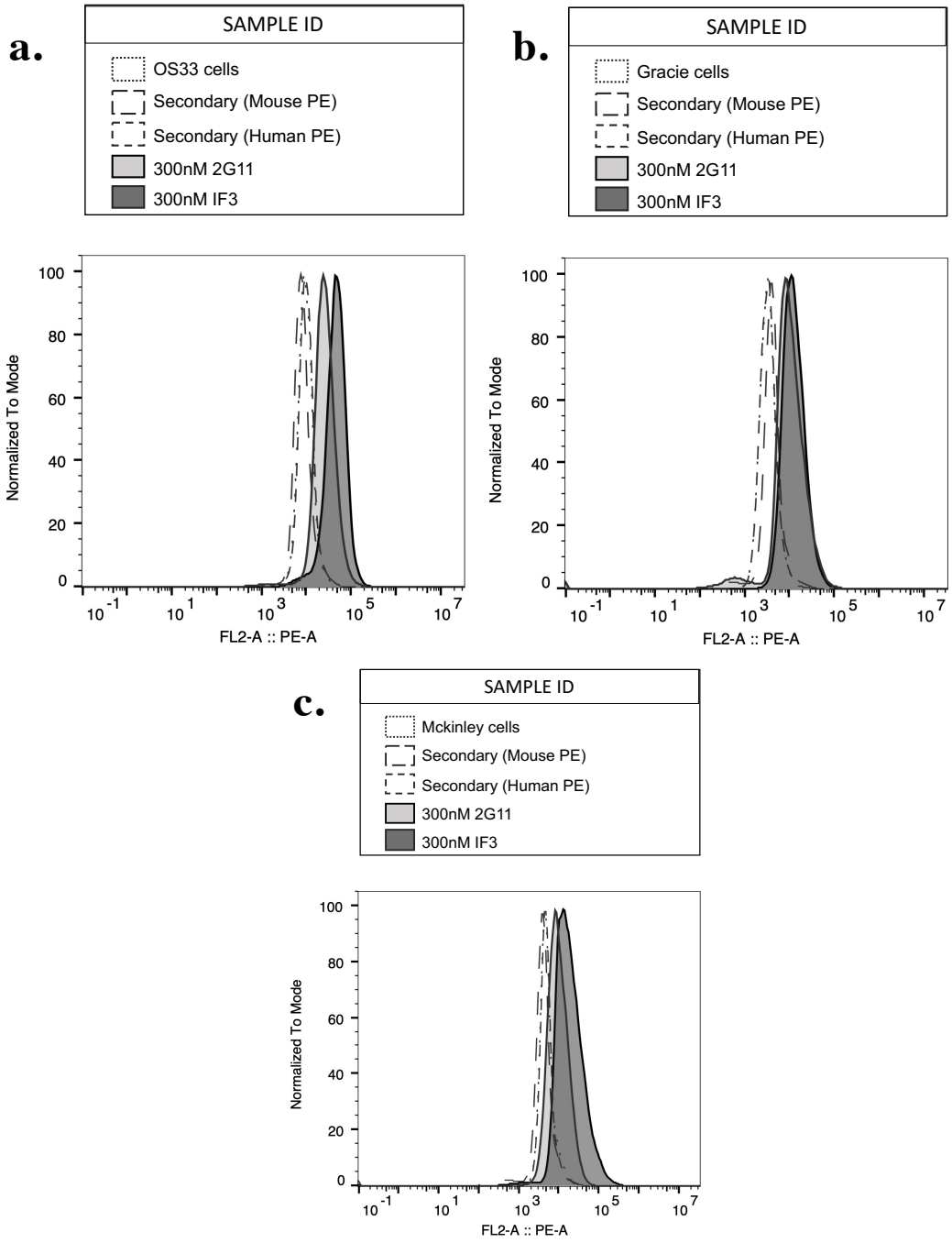

Figure 5.9. Flow cytometry of human and canine OS cells with IF3 antibody. a.) OS33 cells b.) Gracie grafts c.) McKinley. (Broqueza *et al,* 2021)

5.7 Small-scale biodistribution to determine the effect of excess CHXA" (2.5 AND 10 M excess) on the clearance of IF1 and IF3 in the blood

An experiment previously performed in Dr. Dadachova's lab tested the influence of the bifunctional chelator to the blood clearance of an antibody wherein they observed that the higher the molar excess of the linker, the faster the radiolabeled antibody gets cleared from the blood. With this information, we decided to perform a pilot biodistribution study of the IF1 and IF3 antibodies with 2.5 molar excess versus 10 molar excess to determine the effect of the excess CHXA" on the antibodies' blood clearance. Before the biodistribution, ELISA was performed to test whether the conjugation of the antibodies to CHXA" will significantly alter their binding affinity to IGF2R (Figure 5.10). ELISA result shows that conjugated antibodies did not significantly decrease its affinity to IGF2R.

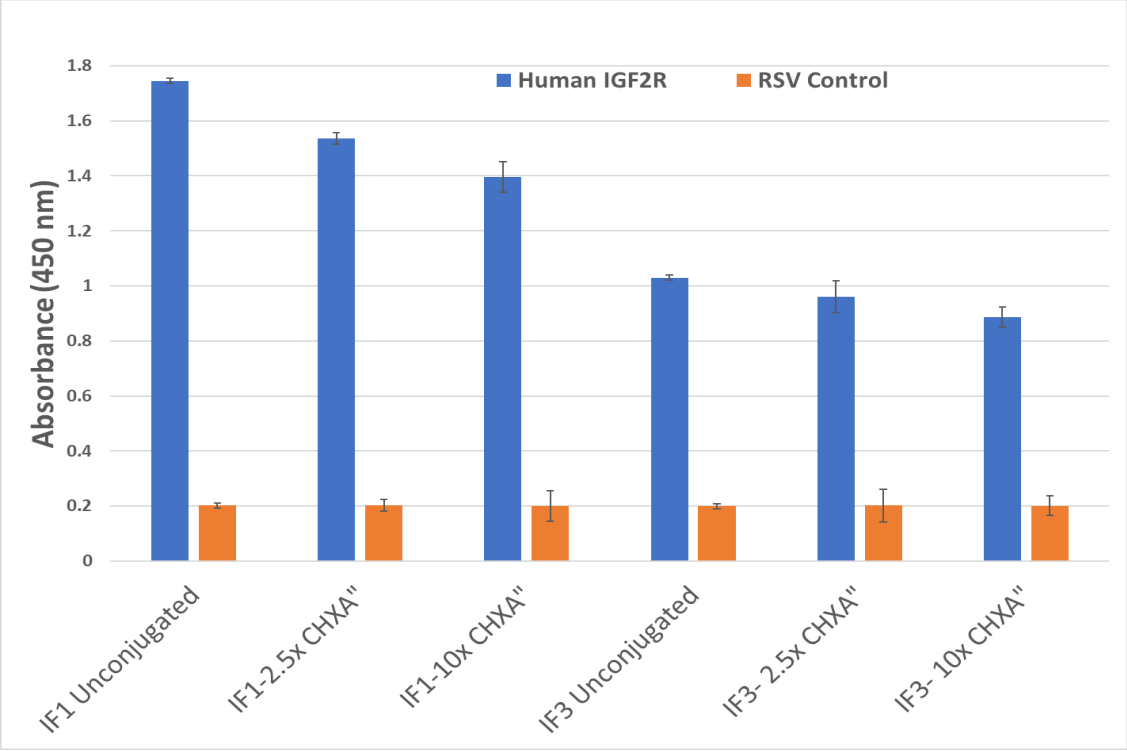

Figure 5.10. ELISA of unconjugated vs conjugated (2.5 M vs 10 M excess of CHXA") of IF1 and IF3 antibodies (Broqueza *et al,* 2021).

The pilot biodistribution shows that IF3 stays in the blood longer than IF1. Moreover, we can confer that the amount of the excess linker plays a role in making the antibody stay in the circulation longer as in both antibodies, the 2.5 M CHXA" excess has a higher %ID/g compared to the 10 M excess. Therefore, we determined to test the IF3 conjugated with 2.5 M excess of CHXA" for imaging. We injected a SCID mouse bearing 143B tumor via intraperitoneal (IP) route with ^{111}In-IF3 and imaged it at 24 hr, 48 hr, and 6 day time point. As seen in figure 5.12, tumor accumulation can be observed at the 48 hr time point as shown by the red circle, highlighting the tumor uptake. Therefore, we moved the project forward using the IF3 antibody and conjugating it with 2.5 M excess of the CHXA" linker for the consecutive experiments.

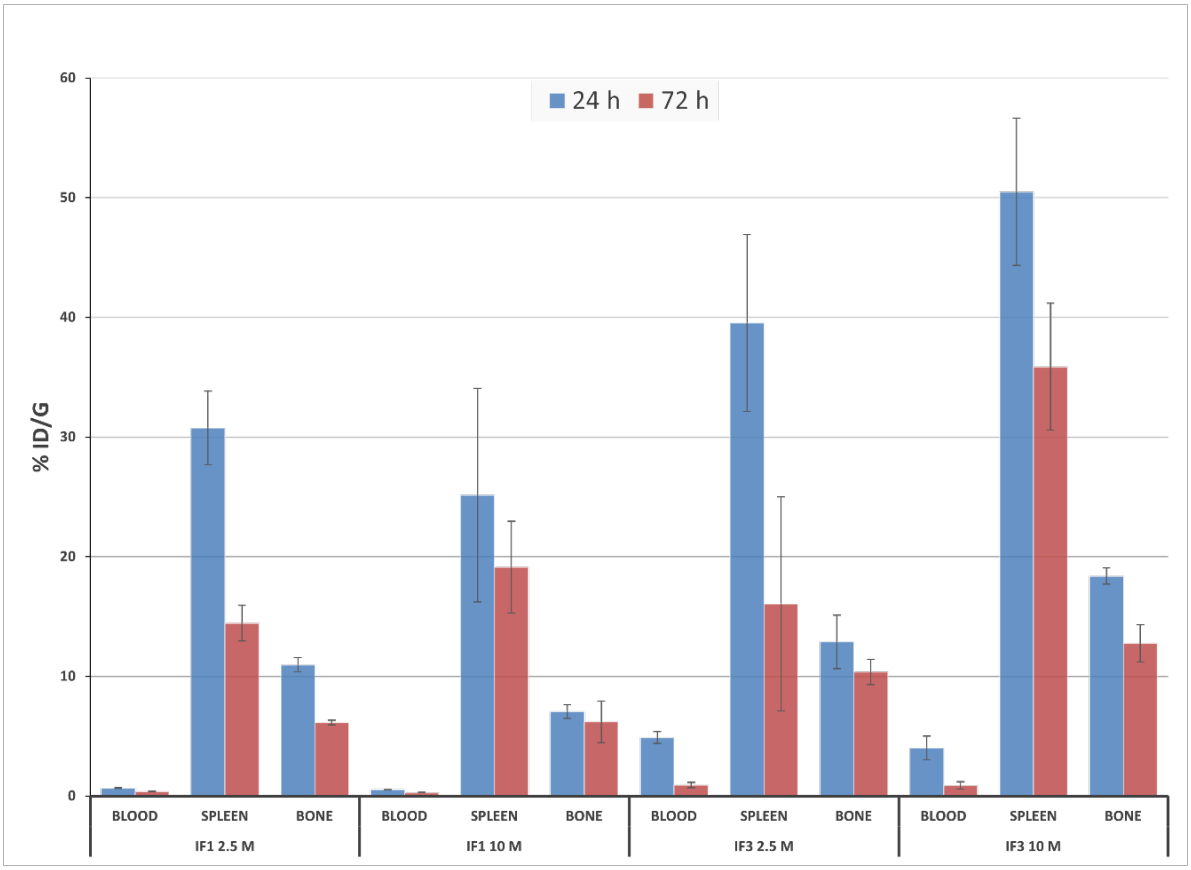

Figure 5.11. Biodistribution of ^{111}In- IF1 vs ^{111}In- IF3 antibodies conjugated with initial 2.5 vs 10 M initial molar excess of CHXA" linker in SCID mice. (Broqueza *et al,* 2021)

The conjugated antibodies were also sent to the University of Alberta mass spectrometry facility to determine the CHXA"/antibody ratio using the matrix-assisted laser desorption/ionization (MALDI) method. MALDI results showed that the IF1-CHXA"-2.5 M and IF1-CHXA"-10 M excess has a CHXA"/antibody ratio of 0.96 and 2.9 respectively whereas IF3-CHXA"-2.5 M and IF3-CHXA"-10 M excess has 0.91 and 3.4.

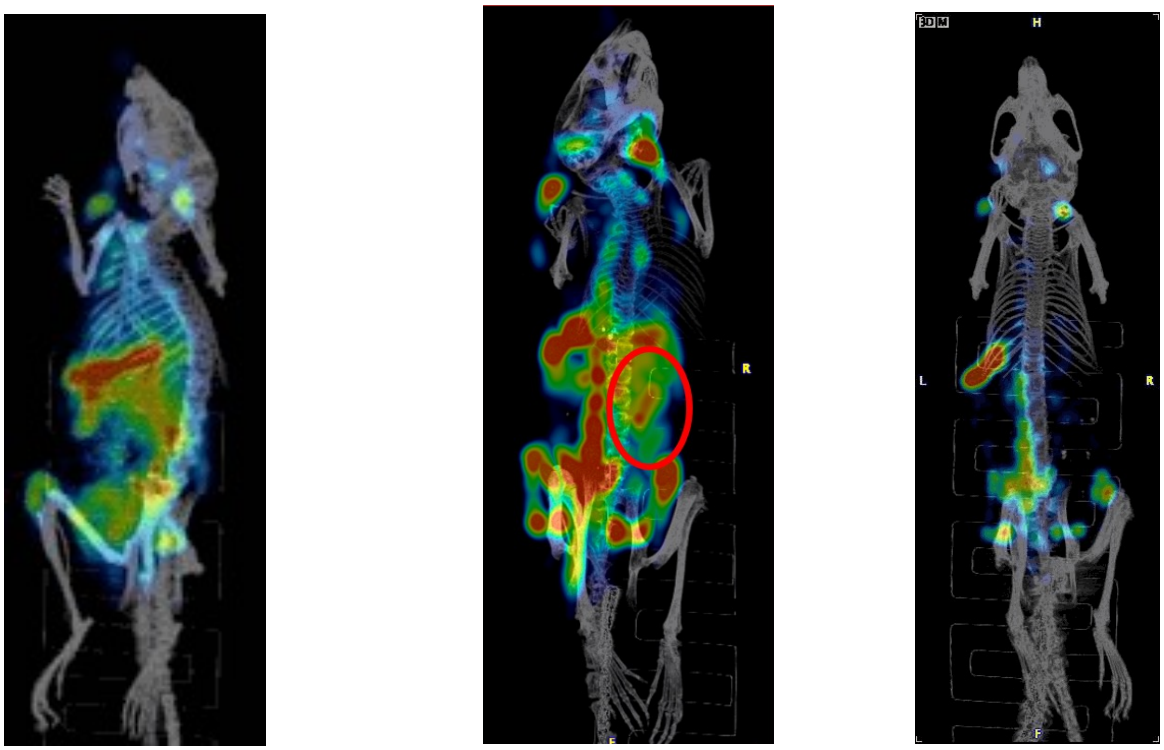

Figure 5.12. MicroSPECT/CT of 143B tumor bearing SCID mice with ^{111}In- labelled IF3 conjugated with initial 2.5 M excess of the CHXA" linker. Tumor is highlighted with a red circle. (Broqueza *et al,* 2021)

5.8 microSPECT/CT of OS33 and Gracie tumor bearing SCID mice labelled with Indium-111 – CHXA" IF3

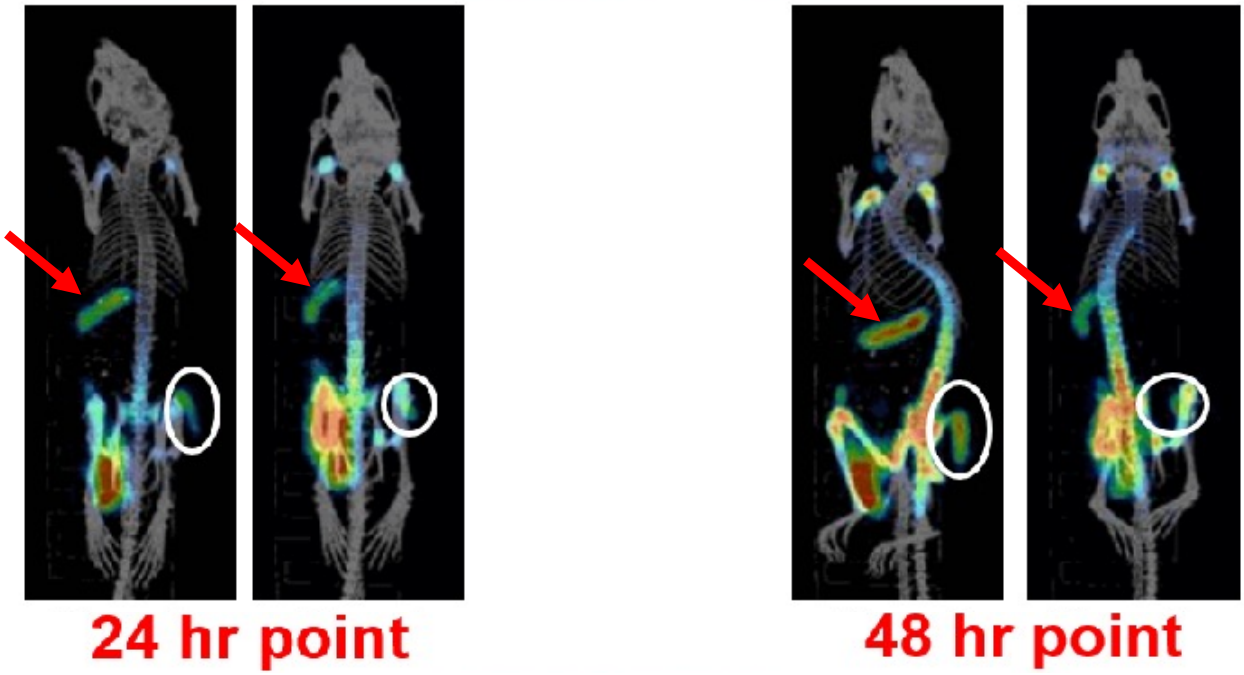

Figure 5.13. MicroSPECT/CT of Gracie tumor bearing SCID mice with ^{111}In- IF3. Tumor accumulation is indicated by the white circles and spleens are indicated by red arrows.

Since we have observed tumor uptake in the SCID mouse bearing the 143B tumor, we went ahead to do another imaging study with the IF3 antibody. Three groups of mice were injected with the human and canine PD cells. Group one was OS33, group 2 was Gracie and group 3 was McKinley. Palpable tumors grew in both OS33 and Gracie groups ~2-3 weeks and were imaged with ^{111}In-IF3 at 24 and 48 hr time point. Unfortunately, no tumors grew in the McKinley group, indicating that the cell line may not be tumorigenic.

In figure 5.13, Gracie mice were injected with the radiolabeled ^{111}In-IF3 via IP route. Tumor accumulation can be observed on the right flank of the mice where the cells were injected. However, significant radioactivity can be observed around the injection site and the spleen was

not showing as much radioactivity as expected which might indicate that the radioactive antibody might have pooled around the site of injection and did not circulate around the body for it to accumulate more on the tumor. Therefore, we decided to inject the next set of mice via IV route to see a clearer image of the tumor accumulation as seen in figures 5.15 and 5.16. We have also performed HPLC as seen in figure 5.14 to test whether the radioactivity observed in figure 5.13 were macroaggregates from the radiolabeled antibody. However, this is not the case as the HPLC data shows that the radiolabeled antibody is pure and has no macroaggregates.

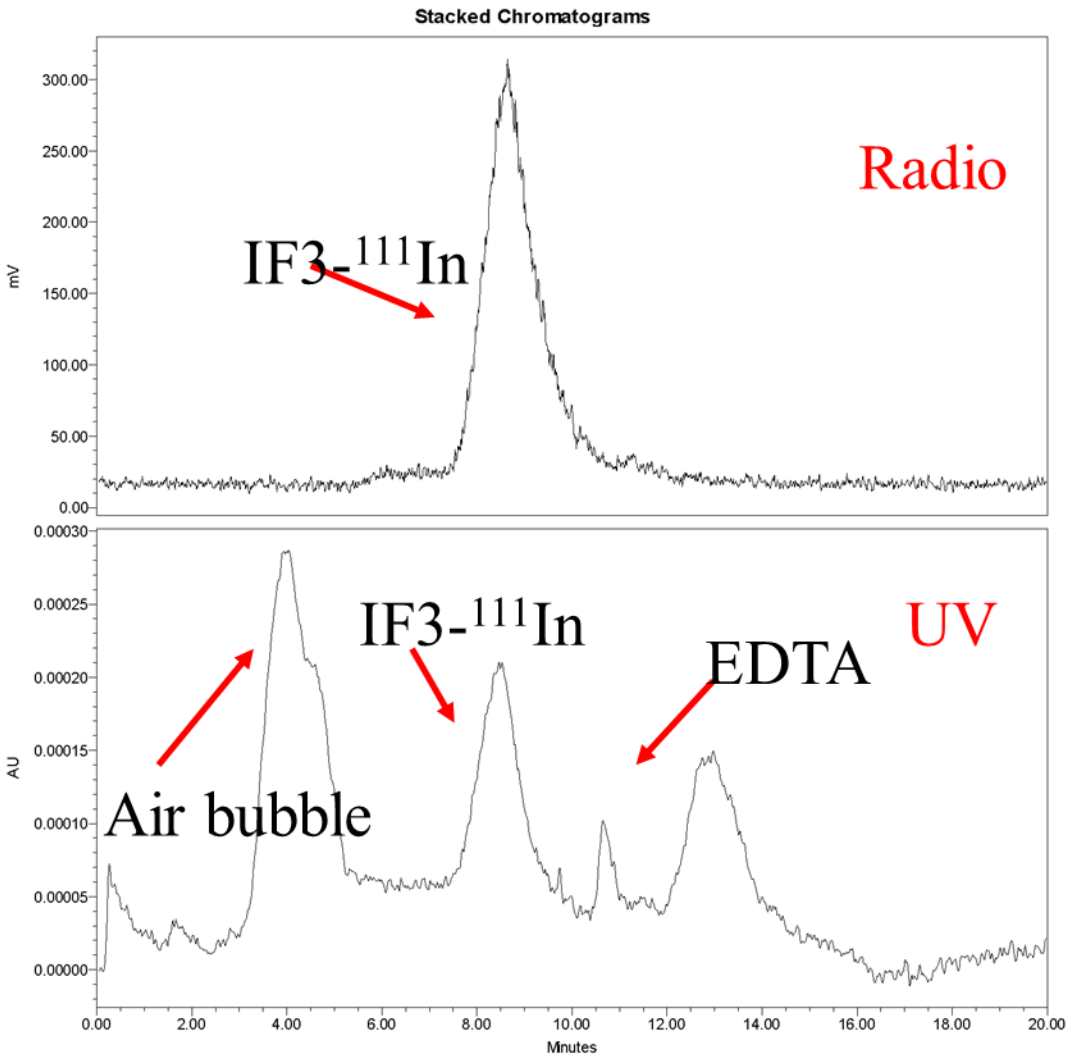

Figure 5.14. RadioHPLC trace of ^{111}In-IF3.

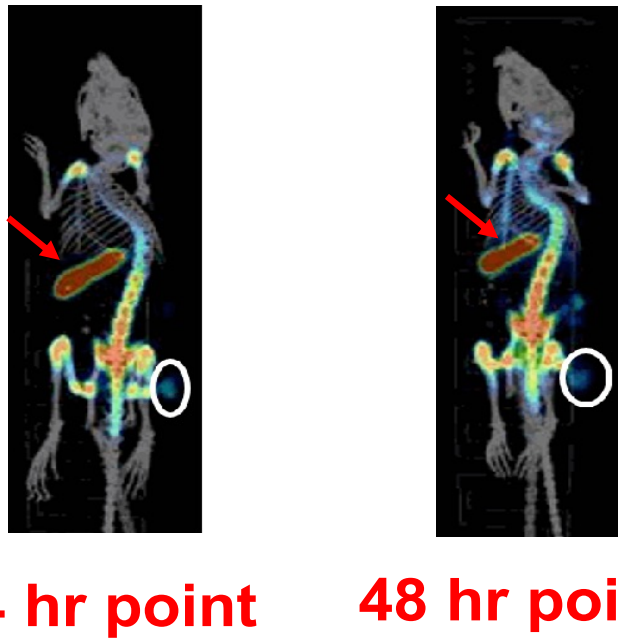

Figure 5.15. MicroSPECT/CT of OS33 tumor bearing SCID mice with ^{111}In- labelled IF3. Tumor accumulation is indicated by the white circles and spleens by the red arrows. (Broqueza *et al,* 2021)

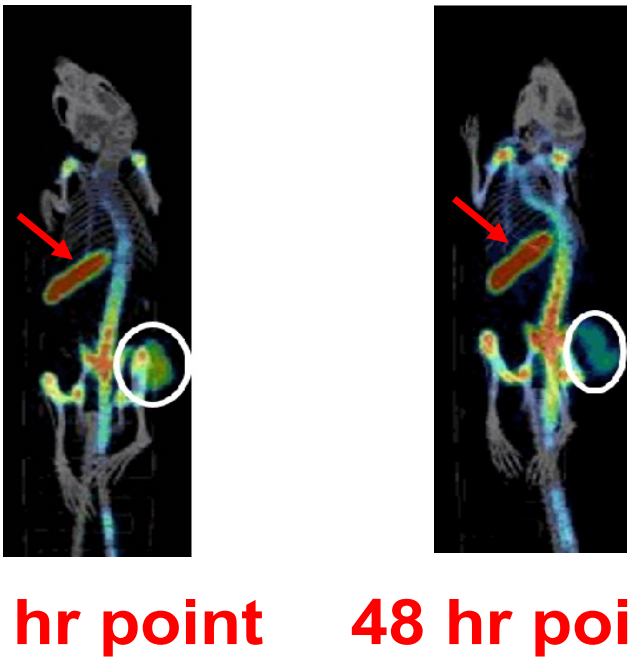

Figure 5.16. MicroSPECT/CT of Gracie tumor bearing SCID mice with ^{111}In- labelled IF3. Tumor accumulation is indicated by the white circles and spleens by the red arrows. (Broqueza *et al,* 2021)

5.9 Radioimmunotherapy study in SCID mice bearing OS33 or Gracie tumor

OS33 tumor bearing mice were randomized into groups of five and Gracie tumor bearing mice were randomized into groups of four. There were four therapy groups for each tumor type. Group 1 was untreated; group 2 received unlabeled IF3 (cold, 12 μg IF3); group 3 received 80 μCi of ^{177}Lu -IF3 (8 μg, 80 μCi); group 4 received 120 μCi of ^{177}Lu -IF3 (12 μg, 120 μCi). Mice were treated with ^{177}Lu- IF3 via IP injection when tumor volume reached approximately 50-100 mm^3. Mice were then monitored by performing tumor measurements and measuring the weights three times a week. In Figure 5.17, the tumor volume was averaged on each day point and normalized by using the formula $(T_n - T_0)/T_0$ where T_0 is the tumor volume at day 0 and T_n at the day of tumor measurement.

	Average Tumor Volume (mm^3)	
	OS33	**Gracie**
Group 1 (Untreated)	63.7213	55.82625
Group 2 (Cold IF3)	52.5299	91.288125
Group 3 (80 μCi Lu-177-IF3)	76.6458	79.895
Group 4 (120 μCi Lu-177-IF3)	61.1318	85.258875

Table 5.1. Average volumes of OS33 and Gracie tumors in SCID mice prior to therapy.

In both therapy studies, there is a continuous growth of the tumors in the untreated and cold groups. For the OS33 groups, there is tumor suppression observed in the treated groups compared to the control groups. Mice in both the 80 μCi and 120 μCi treated group were sacrificed by day 11 as the mice showed symptoms of radiotoxicity and some of the tumors appeared to be necrotic. Two mice from 120 μCi succumbed to radiotoxicity effects by day 11, indicating that 120 μCi is beyond the maximum tolerated dose (MTD). For the Gracie therapy, tumor regression

can be observed by day 2 of the 120 μCi treated group. However, just as in the OS33 group, two mice bearing the Gracie tumor succumbed to radiotoxicity effects in the 120 μCi group. Mice in the Gracie 80 μCi group has also succumbed to radiation side effects and died by day 13. Endpoints of mice were defined by the Humane Intervention Protocol (HIP) and were met by weight loss, lethargy, rapid breathing and abnormal posture. The study was terminated as both treatment groups either met the HIP endpoint or succumbed to radiotoxicity effects.

White blood cells (WBC), red blood cells (RBC), and platelets levels were collected weekly via tail vein puncture (Figure 5.18). WBCs and platelet levels are significantly lower in the treated group compared to the control group by Week 1 in both the OS33 and Gracie group. Moreover, RBC levels of the treated Gracie groups decreased by Week 2. If the OS33 treated groups lasted for another week, it is expected that their RBC levels would also decrease as was observed in an in-house experiment published in 2020 (Malo *et al,* 2020).

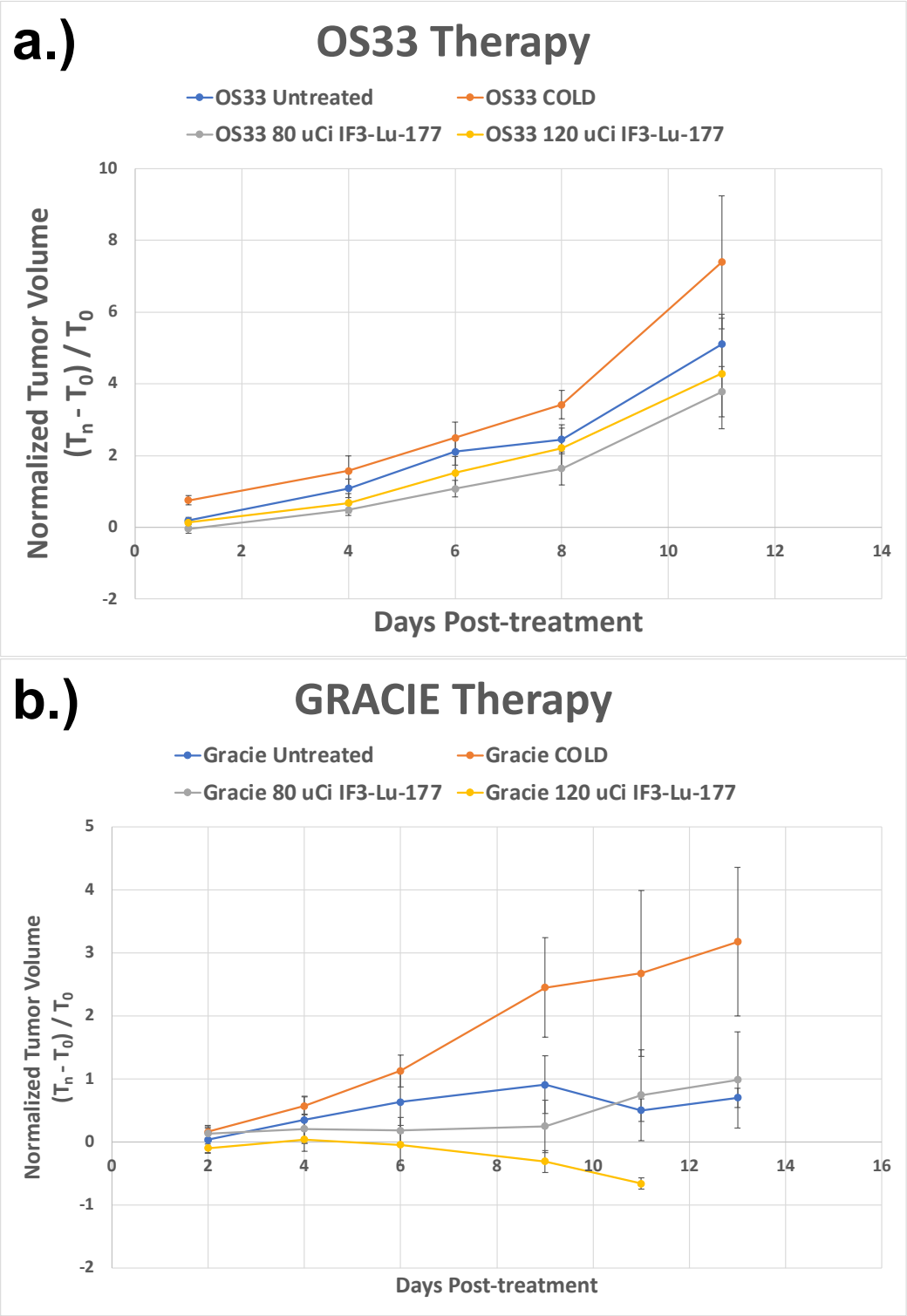

Figure 5.17. Radioimmunotherapy of OS33 (a) and Gracie (b) tumor-bearing SCID mice with ^{177}Lu-IF3. T_0 is the tumor volume at day 0 and T_n at the day of tumor measurement.

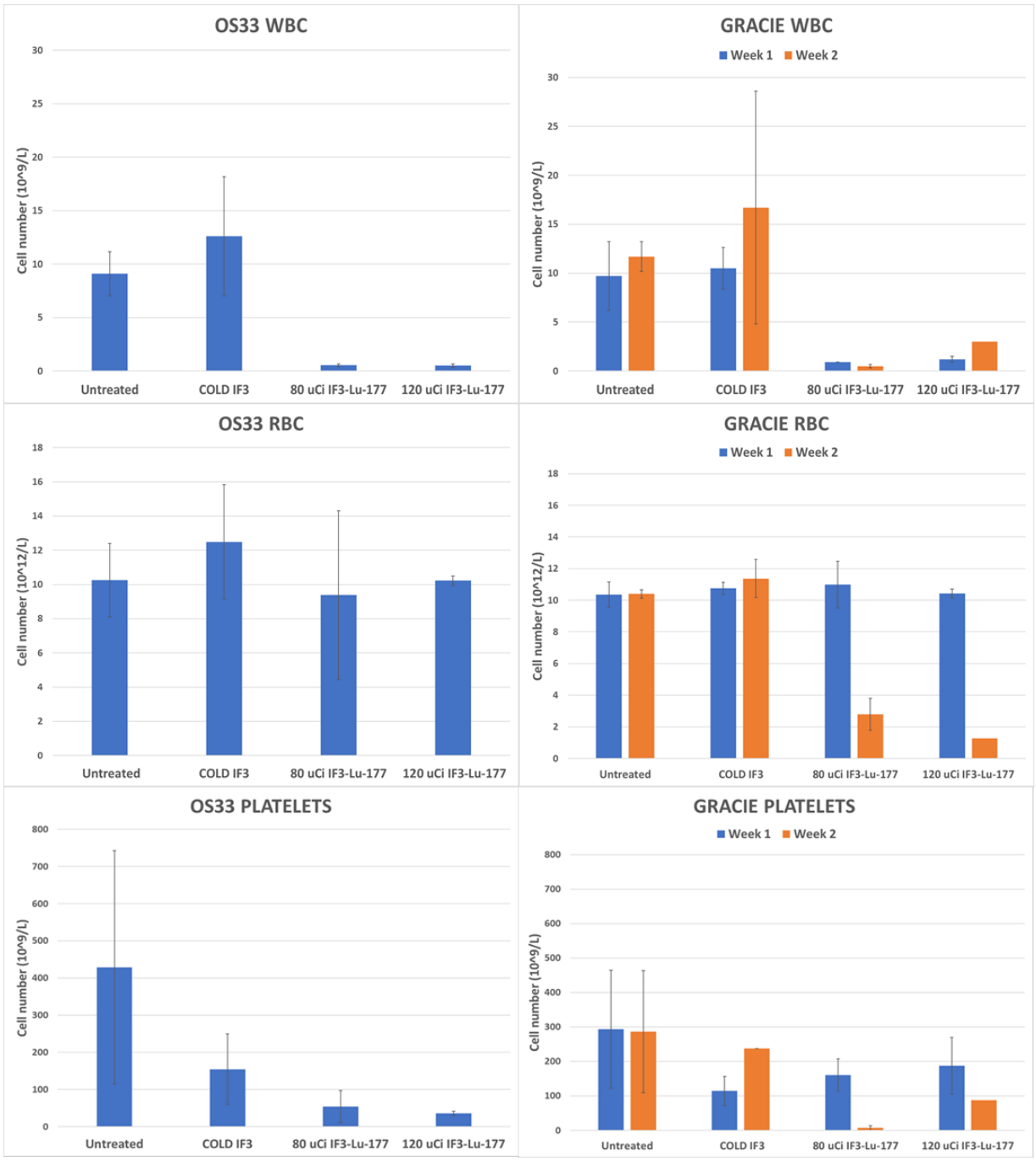

Figure 5.18. Blood cell counts in SCID mice during radioimmunotherapy with 177Lu-IF3.

Gross pathology was also performed on the mice. Blood clotting at the tumor site was observed in both the OS33 and Gracie treated groups. However, the OS33 group showed a more prominent blood clotting (Figure 5.19) which may be due to its higher tumor volume. Red spots in the liver were observed in the 120 µCi groups which may indicate liver damage. Spleens in the 120 µCi treated groups were also significantly smaller compared to the treated once again pointing to the exceeded MTD.

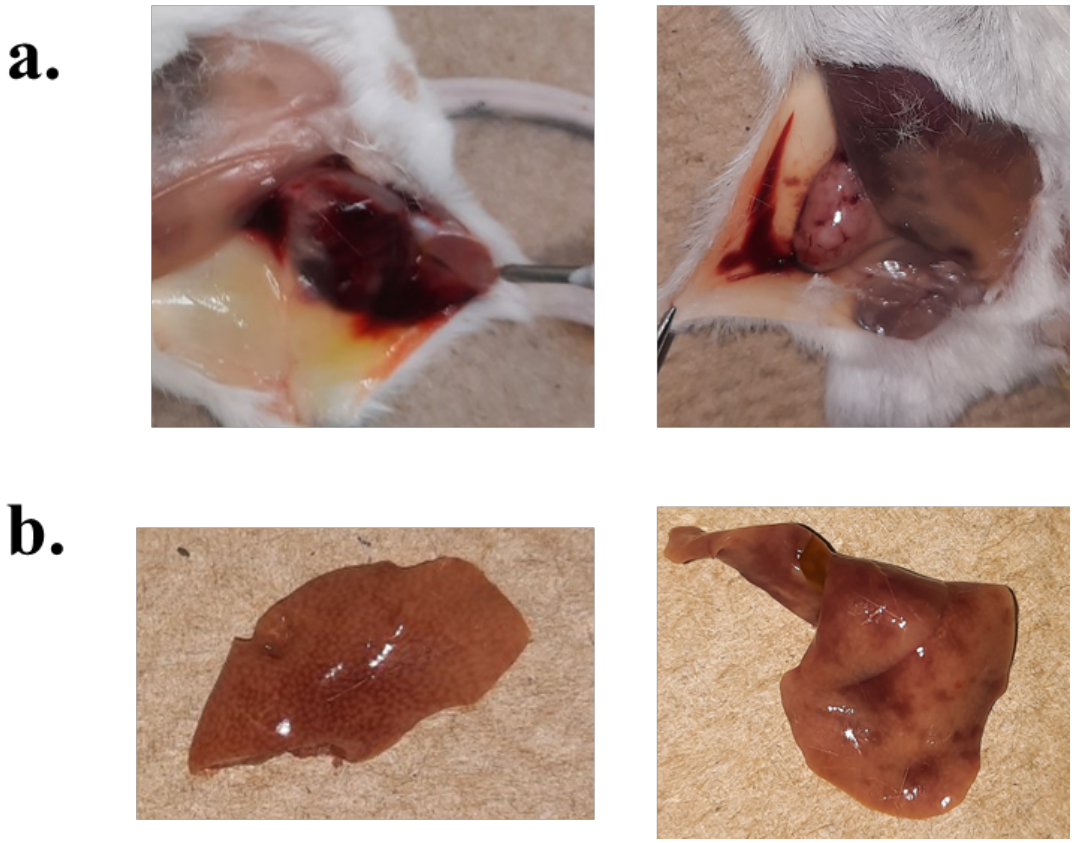

Figure 5.19. Gross pathology of mice treated with 120 µCi ^{177}Lu- IF3. (a) Blood clotting around the tumor area; (b) possible liver damage observed in mice.

6.0 DISCUSSION

The long-term goal of this research project is to develop RIT for the dual treatment of human and canine OS. We aim to achieve this by developing novel fully human antibodies against IGF2R using the phage-display technique with future projects involving caninization of antibodies and development of novel canine antibodies against IGF2R.

IGF2R is a cell surface receptor which modulates the activity of the insulin-like growth factor II (IGF-II) protein by sequestering the growth factor for internalization and degradation as well as lysosomal enzyme sorting. IGF2R was chosen to be the target protein for this project as it has been shown that this protein is overexpressed in human OS cells (Hassan *et al,* 2011) and canine OS tumors (Karkare *et al,* 2019).

To select for IGF2R-specific binders, domains 11-13 of recombinant human, murine and canine IGF2R were expressed and purified. These domains where chosen, as a crystalized structure of the IGF-II/IGF2R complex (Brown *et al,* 2008) shows distinct conserved residues where the ligand interacts with the receptor from domain 11, which acts as the main binding site of IGF-II and domain 13, which facilitates strong ligand receptor interaction. A sequence alignment of the human, murine, and canine IGF-II binding region, containing domains 11-13, showed that this region is highly conserved among these species with 82% sequence identity (Broqueza *et al,* 2021). These domains served as a conserved template for development of antibodies with cross reactivity across the species, enabling a comparative oncology study.

An antibody Fab fragment library developed in Dr. Uppalapati's lab was used to select for IGF2R-specific human mAbs. After several rounds of selection, three leading binders against IGF2R were developed. The binders (hereby known as Fab-1, Fab-2, and Fab-3) were initially

expressed as Fab fragments of the antibodies. We also expressed these antibodies as full-length IgG_1 molecules. After these antibodies were expressed as full-length IgG_1 proteins, the nomenclature of each binder was thereby referred to as IF1 (from Fab-1), IF2 (from Fab-2) and IF3 (from Fab-3). After expression of the antibodies in Expi293F mammalian cells, IF2 yielded low concentrations compared to IF1 and IF3, therefore, the second leading binder was put on hold and the project moved forward using IF1 and IF3.

IF1 and IF3 both demonstrated similar affinity against recombinant IGF2R proteins and bound specifically to different OS cell lines. Non-invasive imaging with microSPECT/CT was initially done in nude mice bearing either OS33 or Gracie tumor. Mice models bearing patient-derived xenografts of human or canine tumor cell lines were desired due to their clinical relevance. This was the rationale for using both the human OS33 and canine Gracie PDXs for tumor imaging and treatment.

IF1 did not show any tumor accumulation in nude mice bearing the human and canine OS tumor at any time point. However, the images demonstrated spleen targeting which was also observed in a previous study as the spleen also expresses IGF2R (Karkare *et al.,* 2019). We hypothesized that the reason for lack of tumor accumulation with IF1 was that the immune system of the nude mice may be suppressing the IGF2R expression on tumors, as these mice are not as immunocompromised as SCID mice. Therefore, we decided to use SCID mice, which lacks both B and T cells, for the induction of OS tumor to confirm the expression of IGF2R for therapy and imaging with IF1 and IF3.

The pharmacokinetics of the radiolabeled IF1 antibody was assessed through a biodistribution study performed in SCID mice bearing human OS 143B tumors. Indium-111, with a half-life of 2.83 days, was used for the biodistribution and imaging studies as it emits

high energy gamma emissions at 173 keV and 247 keV, which are easily visualized on SPECT imaging.

The data from the IF1 biodistribution demonstrated high IF1 blood clearance, but high tumor specificity compared to the 2G11 and RSV controls (Figures 5.7 and 5.8). In the context of imaging agents, fast blood clearance can possibly be an asset with high target to non-target ratio, but excessive clearance in the context of therapy might prevent mAbs from attaining significant tumor uptake and reduce the efficacy of RIT. Due to this, we have decided to test the alternative mAb against IGF2R, IF3. A small-scale biodistribution study comparing the blood clearance of IF1 and IF3 and the influence of the excess bifunctional chelator, CHXA", to the blood clearance of the antibodies showed that minimizing the number of the CHXA" linker molecules helped both antibodies to stay in the circulation longer. This agrees with previous in-house data showing that increased CHXA" linker ratio to mAb increases blood clearance. IF3 also showed a longer blood half-life compared to IF1. Due to this, IF3 conjugated with 2.5 molar excess of the CHXA" linker was used in subsequent experiments. The binding of the IF3 antibody *in vivo* was confirmed by microSPECT/CT imaging which shows tumor accumulation in both OS33 and Gracie mouse models. (Figure 5. 15 and 5.16).

Lutetium-177, a beta-emitting radioisotope with a half-life of 6.7 days, was used for the therapy on SCID mice bearing human and canine OS tumors. Moreover, ^{177}Lu is a theranostic radioisotope, meaning it can be used for imaging due to its gamma emissions and as a therapeutic isotope due to its beta emissions. Two doses of radioactivity, 80 μCi and 120 μCi of ^{177}Lu-IF3 was tested. A low dose of 80 μCi was shown as an effective dose in a previous study (Karkare *et. al.,* 2019). Due to the increased IF3 clearance compared to the commercial anti-IGF2R mAb 2G11, we hypothesized that increasing the dose to 120 μCi may potentially

help increase the efficacy of RIT in the scenario that 80 μCi of ^{177}Lu does not show significant tumor suppression.

For the OS33 groups, there was a continuous tumor growth in both the untreated and cold group. Tumor inhibition was observed in low and high dose ^{177}Lu-IF3-CHXA" in both the human and canine tumor groups. An important note, however, is that the initial tumor volume of the untreated Gracie group was significantly smaller compared to the cold and treated groups and therefore may not fully represent the inhibitory ability of ^{177}Lu-IF3-CHXA". Hence, we based our conclusions of tumor suppression in the treated groups on the cold IF3 treated groups as the initial tumor volume in this group was similar to the treated groups.

Low red and white blood cell counts was observed in all the treated groups which is a common side effect of radioimmunotherapy. Low red and white blood cell counts may be due to the radiation affecting the hematopoietic stem cells in the bone marrow or due to accumulation of radiation in the spleen causing hemolysis. Regrettably, some mice succumbed to radiotoxicity side effects in the high dose 120 μCi ^{177}Lu-IF3 groups, indicating that MTD for this antibody-isotope combination was exceeded. Moreover, gross pathology shows possible sign of liver damage in the 120 μCi groups, clotting issues around the tumor, and a decreased spleen volume.

One possible solution for the future studies to overcome and decrease the number of deaths in the treated groups is to lower the radioactivity dose and to switch to a more radioresistant mice such as nude mice. Co-administration of the cold and the radiolabeled antibody may also increase the efficacy of the therapy as a recently published paper demonstrated co-administration of an unlabeled antibody can increase the efficacy of a therapy (Ponte *et al.,* 2020).

This project holds the promise for RIT as the treatment for OS. However, some limitations should be taken into consideration. The use of severely immunocompromised mice serves as an inherent curb as it voids the immune- mediated response and does not represent a complete mimic of a canine or a human immune system. With this limitation, there is a clear need the need for preclinical models of human or canine tumors in more immunocompetent mice.

Moreover, pharmacokinetics of the antibodies still needs to be assessed especially with the fast blood clearance. The immediate clearance of the antibodies, specifically with IF1, may be explained by target-mediated drug disposition (TMDD) as IGF2R has high expression in spleen of mouse models. The difference between IF1 and IF3 is that the latter has lower affinity towards murine IGF2R. Since we are performing the experiments in mice models, IF3 slightly has a longer half-life in the blood compared to the IF1 antibody which gets degraded out of the system.

High spleen uptake in the imaging experiments can also be a cause of concern in this study. However, a recently published paper (Karkare *et al,* 2019) using RIT for OS have shown that no histological spleen damage, together with no abnormalities in the liver enzymes and kidney biomarkers, can be observed in the RIT treated mice at 80 μCi level.

7.0 CONCLUSION AND FUTURE WORK

With the lack of new effective therapies for OS, RIT presents a promising novel approach to therapy for OS. To date, only unlabeled mAbs for immunotherapy have been evaluated in clinical trials for the therapy of OS. Moreover, in some preclinical studies, ^{153}Samarium-EDTMP or polymeric radiolabeled phosphonates was suggested for targeted therapy of OS.

Novel human antibodies that bind to human, canine and murine IGF2R are promising reagents for further development for RIT of human and canine OS patients.

Future work: Pharmacokinetics and dosimetry of the radiolabelled antibodies still needs to be assessed for RIT. Increasing the half-life of the IF3 antibody in the bloodstream and increasing tumor accumulation may lead to better therapeutic effect. To help decrease major side effects observed in the mice therapy such as blood clotting around the tumor, low blood levels, and a shrunken spleen, a possible solution may be to perform blocking or co-administration of the unlabeled IF3 body with the radiolabeled one. Addressing these issues will hopefully lead to further development of RIT for treatment of human and canine OS patients.

REFERENCES

Almagro, Juan C et al. “Progress and Challenges in the Design and Clinical Development of Antibodies for Cancer Therapy.” Frontiers in immunology vol. 8 1751. 4 Jan. 2018, doi:10.3389/fimmu.2017.01751

Anderson, M., DuBois, S., Gebhardt, M. “Sarcomas of Bone”. Abellof’s Clinical oncology, Elsevier Inc, 2020, , 89, 1604-1654.e8

Bone Cancer (Sarcoma of Bone): Statistics. (January 2021). Retrieved from https://www.cancer.net/cancer-types/bone-cancer-sarcoma-bone/statistics

Broqueza, J.; Prabaharan, C.B.; Andrahennadi, S.; Allen, K.J.H.; Dickinson, R.; MacDonald-Dickinson, V.; Dadachova, E.; Uppalapati, M. Novel Human Antibodies to Insulin Growth Factor 2 Receptor (IGF2R) for Radioimmunoimaging and Therapy of Canine and Human Osteosarcoma. *Cancers* 2021, *13*, 2208. https://doi.org/10.3390/cancers13092208

Brown J, Delaine C, Zaccheo OJ, Siebold C, Gilbert RJ, van Boxel G, Denley A, Wallace JC, Hassan AB, Forbes BE, Jones EY. Structure and functional analysis of the IGF-II/IGF2R interaction. EMBO J. 2008 Jan 9;27(1):265-76. doi: 10.1038/sj.emboj.7601938. Epub 2007 Nov 29. PMID: 18046459; PMCID: PMC2206120.

Brüggemann, Marianne et al. “Human antibody production in transgenic animals.” Archivum immunologiae et therapiae experimentalis vol. 63,2 (2015): 101-8. doi:10.1007/s00005-014-0322-x

Canine Osteosarcoma Fact Sheet. (n.d.). Retrieved from https://vetspecialists.co.uk/fact-sheets-post/canine-osteosarcoma-fact-sheet/.

Castelli, María Sofía et al. “The pharmacology and therapeutic applications of monoclonal antibodies.” Pharmacology research & perspectives vol. 7,6 (2019): e00535. doi:10.1002/prp2.535

Czarnecka, A. M., Synoradzki, K., Firlej, W., Bartnik, E., Sobczuk, P., Fiedorowicz, M., Grieb, P., & Rutkowski, P. (2020). Molecular Biology of Osteosarcoma. *Cancers*, *12*(8), 2130. https://doi.org/10.3390/cancers12082130

Davies Veterinary Specialists, Manor Farm Business Park, Higham Gobion, Herts SG5 3HR 01582 853878 ©2018 Davies Veterinary Specialists Limited

Davis AM, Bell RS, Goodwin PJ. Prognostic factors in osteosarcoma: a critical review. J Clin Oncol. 1994 Feb;12(2):423-31. doi: 10.1200/JCO.1994.12.2.423. PMID: 8113851.

Dawe J. (2007). Osteosarcoma in a 6-year-old Newfoundland dog: limb-sparing surgery and cisplatin chemotherapy. *The Canadian veterinary journal = La revue veterinaire canadienne*, *48*(11), 1169–1171.

Doevendans, Erik, and Huub Schellekens. “Immunogenicity of Innovative and Biosimilar Monoclonal Antibodies.” Antibodies (Basel, Switzerland) vol. 8,1 21. 5 Mar. 2019, doi:10.3390/antib8010021

Ehrhart, N., Ryan, S., Fan, T. “Tumors of the Skeletal System”. Withrow and MacEwen's Small Animal Clinical Oncology. Edited by Stephen J. Withrow, David M. Vail and Rodney L. Page. Elsevier Inc. 2013. pp. 463-500

FDA-approved radiopharmaceuticals. (n.d.), Retrieved from https://www.cardinalhealth.com/en/product-solutions/pharmaceutical-products/nuclear-medicine/safety-and-compliance/fda-approved.html

Fellouse, F. A., and Sidhu, S. S. (2007) Making antibodies in bacteria, In Making and using antibodies: A practical handbook (Howard, G. C., and Kaser, M. R., Eds.), pp 157- 180, CRC Press, Boca Raton, FL.

Geller, David S et al. "Targeted therapy of osteosarcoma with radiolabeled monoclonal antibody to an insulin-like growth factor-2 receptor (IGF2R)." Nuclear medicine and biology vol. 43,12 (2016): 812-817. doi:10.1016/j.nucmedbio.2016.07.008

Green, Damian J, and Oliver W Press. "Whither Radioimmunotherapy: To Be or Not To Be?." Cancer research vol. 77,9 (2017): 2191-2196. doi:10.1158/0008-5472.CAN-16- 2523

Grimer RJ, Taminiau AM, Cannon SR (2002) Surgical outcomes in osteosarcoma. J Bone Joint Surg Br 84, 395–400.

Hassan, S. E. et al. Cell surface receptor expression patterns in osteosarcoma. Cancer 118, 740– 9 (2012).

Imran H, Enders F, Krailo M, Sim F, Okuno S, Hawkins D, Neglia J, et al. (2009) Effect of time to resumption of chemotherapy after definitive surgery on prognosis for nonmetastatic osteosarcoma. J Bone Joint Surg Am 91, 604–612.
John W. Kehoe and and Brian K. Kay*. Filamentous Phage Display in the New Millennium. Chemical Reviews 2005 105 (11), 4056-4072 DOI: 10.1021/cr000261r.

Karkare, S., Allen, K.J.H., Jiao, R. et al. Detection and targeting insulin growth factor receptor type 2 (IGF2R) in osteosarcoma PDX in mouse models and in canine osteosarcoma tumors. Sci Rep 9, 11476 (2019) doi:10.1038/s41598-019-47808-y

Laube, F. Mannose-6-phosphate/insulin-like growth factor-II receptor in human melanoma cells: effect of ligands and antibodies on the receptor expression. Anticancer Res. 29, 1383–8 (2009).

Lerner, R. Combinatorial antibody libraries: new advances, new immunological insights. Nat Rev Immunol 16, 498–508 (2016) doi:10.1038/nri.2016.67

Maeda, J., Yurkon, C. R., Fujisawa, H., Kaneko, M., Genet, S. C., Roybal, E. J., Rota, G. W., Saffer, E. R., Rose, B. J., Hanneman, W. H., Thamm, D. H., & Kato, T. A. (2012). Genomic instability and telomere fusion of canine osteosarcoma cells. PloS one, 7(8), e43355. https://doi.org/10.1371/journal.pone.0043355

Makielski KM, Mills LJ, Sarver AL, Henson MS, Spector LG, Naik S, Modiano JF. Risk Factors for Development of Canine and Human Osteosarcoma: A Comparative Review. Vet Sci. 2019 May 25;6(2):48. doi: 10.3390/vetsci6020048. PMID: 31130627; PMCID: PMC6631450.

Malo ME, Allen KJH, Jiao R, Frank C, Rickles D, Dadachova E. Mechanistic Insights into Synergy between Melanin-Targeting Radioimmunotherapy and Immunotherapy in Experimental Melanoma. Int J Mol Sci. 2020 Nov 18;21(22):8721. doi: 10.3390/ijms21228721. PMID: 33218169; PMCID: PMC7698872.

Meyer J.S., Nadel H.R., Marina N. et al. Imaging guidelines for children with Ewing sarcoma and osteosarcoma: a report from the Children‘s Oncology Group Bone Tumor Committee. *Pediatr Blood Cancer*. 2008; 51: 163-170

Milenic DE, Brady ED, Brechbiel MW. Antibody-targeted radiation cancer therapy. Nat Rev Drug Discov 2004; 3(6):488–99.

Mirabello, Lisa et al. “International osteosarcoma incidence patterns in children and dolescents, middle ages and elderly persons.” International journal of cancer vol. 125,1 (2009): 229-34. doi:10.1002/ijc.24320

Misaghi, Amirhossein et al. “Osteosarcoma: a comprehensive review.” *SICOT-J* vol. 4 (2018): 12. doi:10.1051/sicotj/2017028.

Mueller F, Fuchs B, Kaser-Hotz B. Comparative biology of human and canine osteosarcoma. Anticancer Res. 2007 Jan-Feb;27(1A):155-64. PMID: 17352227.

Nagarajan, R., Kamruzzaman, A., Ness, K. K., Marchese, V. G., Sklar, C., Mertens, A., Yasui, Y., Robison, L. L., & Marina, N. (2011). Twenty years of follow-up of survivors of childhood osteosarcoma: a report from the Childhood Cancer Survivor Study. Cancer, 117(3), 625–634. https://doi.org/10.1002/cncr.25446

Osteosarcoma - Childhood and Adolescence: Diagnosis. (August 2019). Retrieved from https://www.cancer.net/cancer-types/osteosarcoma-childhood-and-adolescence/diagnosis.

Osteosarcoma - Childhood and Adolescence: Introduction. (August 2019). Retrieved from https://www.cancer.net/cancer-types/osteosarcoma-childhood-and-adolescence/introduction.

Osteosarcoma - Childhood and Adolescence: Risk Factors. (August 2019). Retrieved from https://www.cancer.net/cancer-types/osteosarcoma-childhood-and-adolescence/risk-factors.

Osteosarcoma - Childhood and Adolescence: Statistics. (February 2021). Retrieved from https://www.cancer.net/cancer-types/osteosarcoma-childhood-and-adolescence/statistics

Osteosarcoma: An Introduction, (October 2012n.d.). Retrieved from http://sarcomahelp.org/osteosarcoma.html.

Ponte JF, Lanieri L, Khera E, Laleau R, Ab O, Espelin C, Kohli N, Matin B, Setiady Y, Miller ML, Keating TA, Chari R, Pinkas J, Gregory R, Thurber GM. Antibody Co-Administration Can Improve Systemic and Local Distribution of Antibody-Drug Conjugates to Increase *In Vivo* Efficacy. Mol Cancer Ther. 2021 Jan;20(1):203-212. doi: 10.1158/1535-7163.MCT-20-0451. Epub 2020 Nov 11. PMID: 33177153; PMCID: PMC7790875.

Poon AC, Matsuyama A, Mutsaers AJ. Recent and current clinical trials in canine appendicular osteosarcoma. Can Vet J. 2020 Mar;61(3):301-308. PMID: 32165755; PMCID: PMC7020630.

Raymond AK, Jaffe N (2009) Osteosarcoma multidisciplinary approach to the management from the pathogist's perspective, in Pediatric and Adolescent Osteosarcoma. p. 3–13

Ritter J, Bielack SS. Osteosarcoma. Ann Oncol. 2010 Oct;21 Suppl 7:vii320-5. doi: 10.1093/annonc/mdq276. PMID: 20943636.

Ryman JT, Meibohm B. Pharmacokinetics of Monoclonal Antibodies. CPT Pharmacometrics Syst Pharmacol. 2017 Sep;6(9):576-588. doi: 10.1002/psp4.12224. Epub 2017 Jul 29. PMID: 28653357; PMCID: PMC5613179.

Sachdev, S.S. & Frederic, A.F. Making Antibodies in Bacteria. in Making and Using Antibodies 157-180 (CRC Press, 2006).

Savage, S.A.;Woodson, K.;Walk, E.; Modi,W.; Liao, J.; Douglass, C.; Hoover, R.N.; Chanock, S.J. Analysis of Genes Critical for Growth Regulation Identifies Insulin-like Growth Factor 2 Receptor Variations with Possible Functional Significance as Risk actors for Osteosarcoma. Cancer Epidemiol. Biomark. Prev. 2007, 16, 1667–1674.

Sgouros, G., Bodei, L., McDevitt, M.R. et al. Radiopharmaceutical therapy in cancer: clinical advances and challenges. Nat Rev Drug Discov 19, 589–608 (2020). https://doi.org/10.1038/s41573-020-0073-9

Sharkey RM, Goldenberg DM. Perspectives on cancer therapy with radiolabelled monoclonal antibodies. J Nucl Med 2005; 46(Suppl. 1):115S–27S.

Simpson, S., Dunning, M. D., de Brot, S., Grau-Roma, L., Mongan, N. P., & Rutland, C. S. (2017). Comparative review of human and canine osteosarcoma: morphology, epidemiology, prognosis, treatment and genetics. *Acta veterinaria Scandinavica*, *59*(1), 71. https://doi.org/10.1186/s13028-017-0341-9

Stoewen, D. and Pinard, C. (n.d.). Osteosarcoma in Dogs. Retrieved from https://vcacanada.com/know-your-pet/osteosarcoma-in-dogs.

Vazquez-Lombardi R, Nevoltris D, Luthra A, Schofield P, Zimmermann C, Christ D. Transient expression of human antibodies in mammalian cells. Nat Protoc. 2018 Jan;13(1):99-117. doi: 10.1038/nprot.2017.126. Epub 2017 Dec 14. PMID: 29240734.
ved.html.

Vidarsson, Gestur et al. "IgG subclasses and allotypes: from structure to effector functions." Frontiers in immunology vol. 5 520. 20 Oct. 2014, doi:10.3389/fimmu.2014.00520

What You Should Know about Osteosarcoma (Bone Cancer) in Dogs. (n.d.) Retrieved from https://petcureoncology.com/what-you-should-know-about-osteosarcoma-bone-cancer-in dogs/#:~:text=Signs%20and%20Symptoms%20of%20Osteosarcoma%20in%20Dogs&text= Swelling%20or%20a%20mass%3B%20this,difficulties%20or%20lameness%20with%20rib.

Zaheer, Javeria et al. "Combination Radioimmunotherapy Strategies for Solid Tumors." International journal of molecular sciences vol. 20,22 5579. 8 Nov. 2019, doi:10.3390/ijms20225579